Battery State-of-Charge Estimation Using Neural Networks

Chenyao Liao

Submitted in partial fulfillment of the
requirements for the degree of
Master of Science
under the Executive Committee
of the Graduate School of Arts and Sciences

COLUMBIA UNIVERSITY

2019

Abstract

Battery State-of-Charge Estimation Using Neural Networks

Chenyao Liao

This thesis proposes a way to augment the existing machine learning algorithm applied to state-of-charge estimation by introducing a form of pulse injection to the running battery cells. It is believed that the information contained in the pulse responses can be interpreted by a machine learning algorithm whereas other techniques are difficult to decode due to the nonlinearity. OCV Mapping is also applied in order to evaluate and compare the performances with feedforward neural network (FNN) -based approach. Coulomb-counting is selected as the basis of making comparison as it is capable of obtaining the SoC with an error less than 0.1%. The detailed system layout is given to perform the augmented SoC estimation integrated in a real-world testbench. Testing procedures specifically designed for both OCV Mapping and FNN-based approach are also explained and provided. A 2-hidden layer FNN is trained to acquire the nonlinear relationship between the training pulse and the ground-truth SoC. The experimental data is trained and the results are shown within 6-8mins computation time and an error boundary of 1.13% for charge and 0.80% for discharge, whereas OCV Mapping has approximately 3.35% SoC estimation error for charge and 1.86% for discharge even after 90 minutes relaxation.

Table of Contents

List of Graphs

List of Charts

Acknowledgments

I would like to thank Professor Matthias Preindl for his guidance and continuous support through each stage of the process, for sharing the access to his GPU, which saved me a lot of time on the training of FNNs, for giving me the opportunity to join MPLab, inspiring my interest in BMS technologies and always be kind and encouraging.

My sincere thanks also go to PhD candidate Weizhong Wang, who was instrumental in defining the path of my research and provided insight and expertise that greatly assisted the research. I would also like to thank my research partner, Youssef Amr Fahmy, for constructing the FNN and sharing his illuminating views on a number of issues related to the project.

Without they precious support it would not be possible to conduct this research.

Chapter 1: Introduction

1.1 Development of Electric Vehicles

Due to the environmental impact of the petroleum-based transportation infrastructure and the development of renewable energy, the electric transportation infrastructure has seen its resurgence for last decades. Electric vehicles (EVs) are considered as Green and environmental-friendly as the electric power that it consumes can be generated from a wide range of sources, such as fossil fuels, nuclear power and various kinds of renewable energy. This would heavily cut the fuel consumption and gas emission, also would reinforce the secure level of energy usage via geographic diversification of the available energy sources. (Eberle and Helmolt, 2010)

The development of electric vehicle has a long history. (Situ, 2009; Chan, 2002) The first EV debuted in U.S. as early as 1890s, which was regarded as one of the earliest automobiles and its development was way ahead of combustion engine from late 1920s to 1930s. Inherited from horse carriages, it was the major transportation tool of the time that widely used in the society and playing a vital role in land transportation However, the development of EV is full of obstructions. From 1930s, the market was overtaken by gasoline vehicles, which can be mass produced at a lower cost. Petrol also became a cheap power source for transportation with new technologies. Since then, the gas-powered vehicles surpassed EV both in performance and cost, the production and development of EV came to a halt.

Not until the last decade did EV see its revival with a great exponentially increasing deal of demand. According to data from International Energy Agency, the amount of global new electric cars sales grows from 2.24 thousand in 2008 to 1.98 million in 2018. Experts believes the demand of EV is still growing. Deloitte, a famous auditing and consulting company, estimated this number would double to 4 million in 2020 and become 21 million in 2030

(Woodward, 2018). The outlook for annual global EV sales, along with projections from 2018-2030 is shown in Fig. 1, as well as the market share of EV.
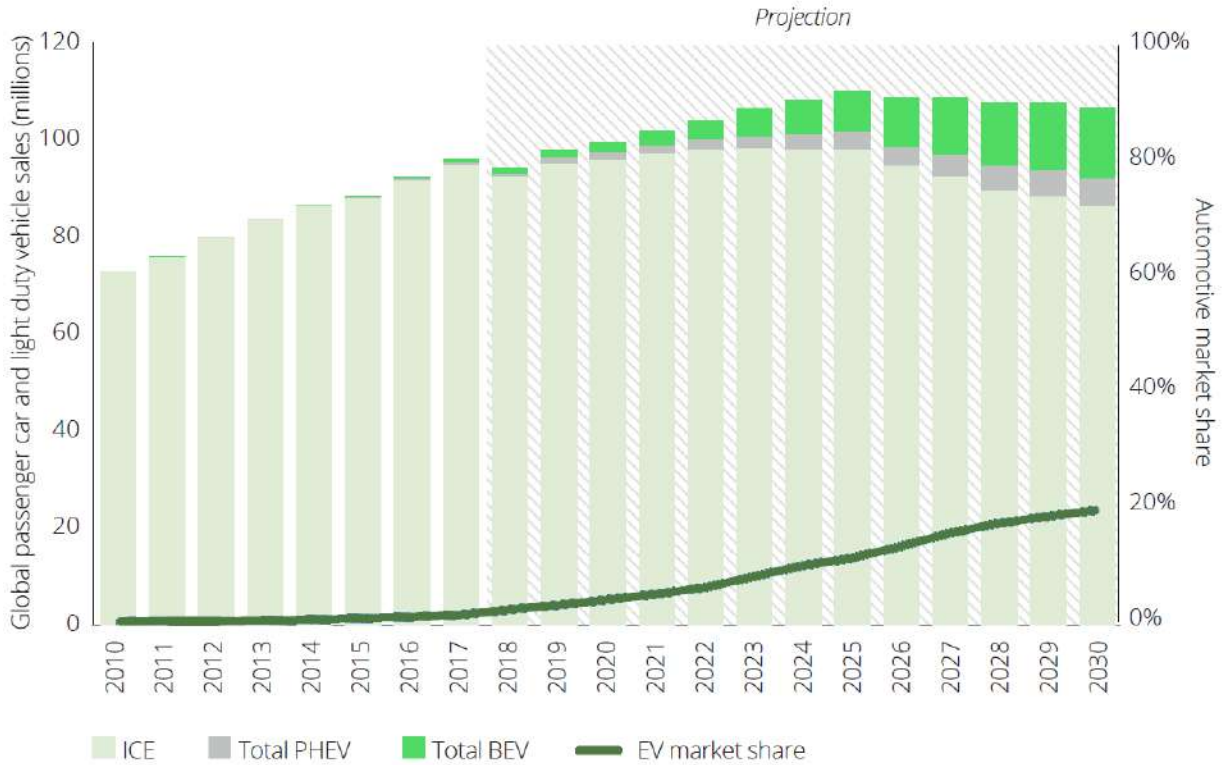
Figure 1: The projection of increasing EV market share. [1]

Policies and regulations play a critical role in the emerging market. Most of major countries set emissions targets and plan to replace gasoline and diesel vehicles with EV. EU, for example, should raise EV share to 10 percent by 2025 in order to meet its own carbon dioxide emission target. Incentive policies are adopted to encourage purchase of EV, including government subsidies and tax exemptions, which promote EV sales in multiple regions. Fig. 2 illustrates EV annual passenger car and light duty vehicle sales in major regions.

---

[1] Data from International Energy Agency (IEA), IHS, Deloitte analysis (2018).
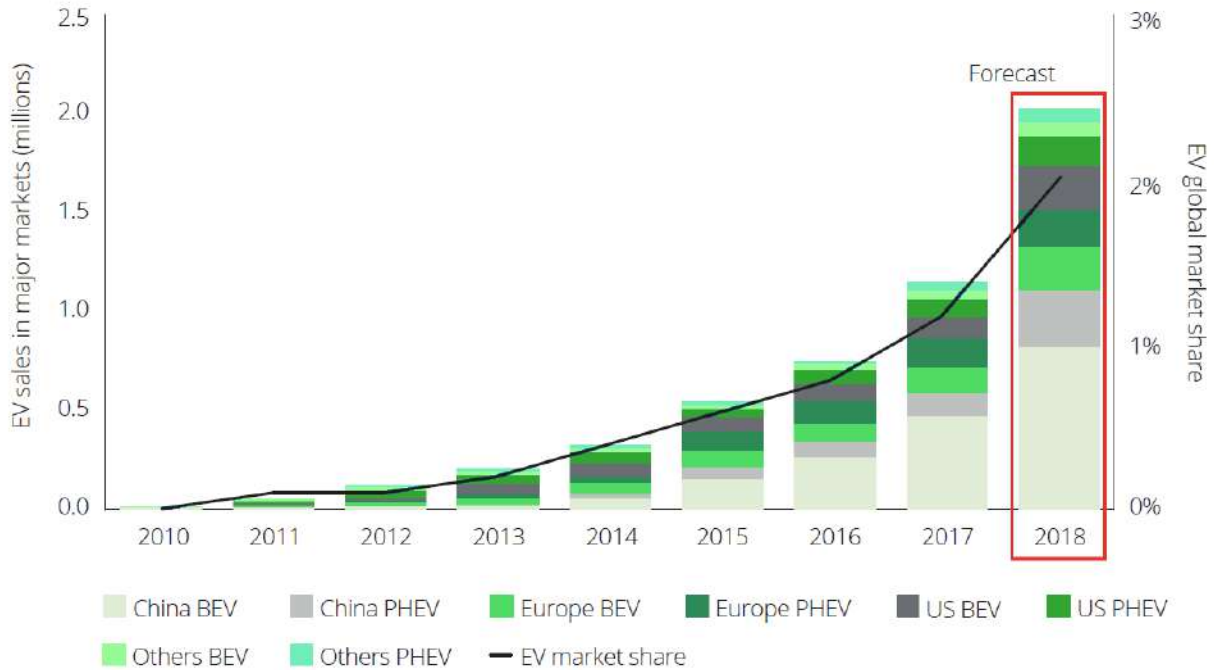
Figure 2: EV annual passenger car and light duty vehicle sales in major regions.[2]

In addition to the government incentives, consumers are important factor in EV market. With a raising awareness of protecting environment, EVs meet the demand of consumers with green energy and lower noise during driving. The consumers are expecting more advanced battery technologies, which would greatly increase driving range of EV as well as fasten the speed of charging batteries. With the development of new techniques, customers would more and more turn to EV instead of gasoline vehicles.

1.2 Motivation

There are three main categories of electric vehicles (EVs) (Carley, 2014), classified by sources they apply. (1) BEVs, or battery electric vehicles are vehicles that only use rechargeable batteries as power supply. (2) HEVs, or hybrid electric vehicles use both electric power and gasoline. (3) PHEVs of plug-in hybrid electric vehicles, also use electric power and gasoline,

---

[2] Data from International Energy Agency (IEA), HIS (2018).

while it has an external electrical power source. All of them mentioned above are more or less powered by battery packs.

The battery, as a crucial core element of electric vehicles, its development has also been renewed. Lithium-ion batteries (LiB) have a promising future in this realm due to its high energy density, long cyclability and low self-discharge rate characteristics. (Dunn et al., 2011; Li et al., 2019) The high energy density allows the Lithium-ion batteries to store six times of energy as can be stored in Lead acid battery. Additionally, over a thousand of charge/discharge cycles can be handled by LiB, whereas the Lead acid battery is only able to handle less than 500 cycles. Furthermore, the charge loss of LiB is as low as 5% per month, while the Nickel–Metal Hydride (NIMH) battery has a 20% charge loss per month. The development of EVs, UPS, mobile phone and smart grid therefore have heavy dependence on LiB technology (Zaghib et al., 2015).

The motivation of this thesis basically arises from the real-world EV applications. In the development of EV, safety issues are undoubtedly a top priority, especially the safety of battery pack. In order to make sure the battery packs are in a healthy state when the EV is driving, it is necessary to monitor some key characteristics that could represent the health status of the battery. For instance, a moving EV stops at a red light, those characteristics are expected to be obtained during this stop period. A battery management system (BMS) functions as a system that take care of the battery packs by monitoring their states, meanwhile, communicate with other onboard subsystems, as depicted in Fig. 3.
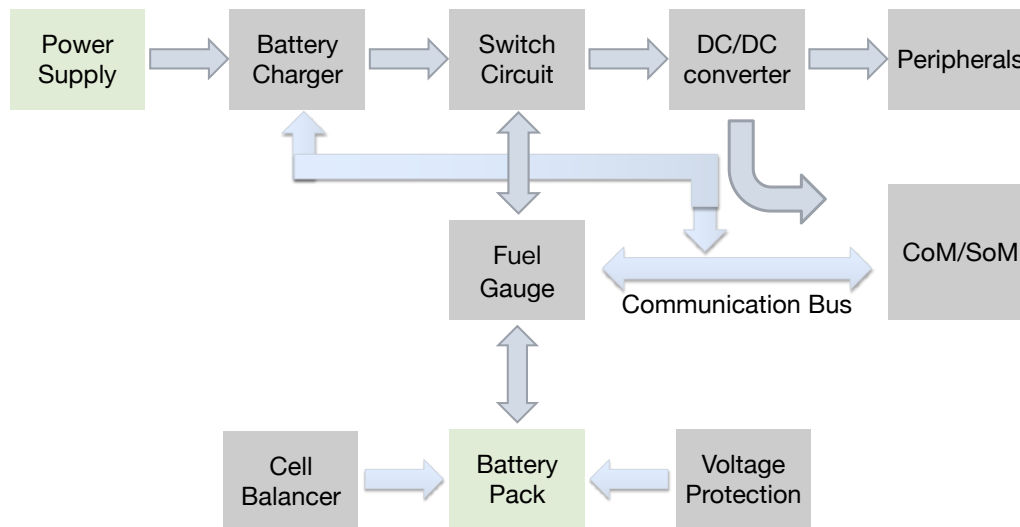
Figure 3: Overview of Battery Management System (BMS).

The purpose of the battery management system is to control and charge the battery pack, provide overvoltage or undervoltage protection, as well as communicate with onboard peripherals. It contains the battery charger, switch circuit, DC/DC converter, etc. The cell balancer module is used to control the batteries in the battery pack in order to realize battery balancing, voltage protection module can set the upper- and lower-bound limit for battery to prevent the battery from being overcharged or undercharged. (Cheng et al., 2011; Rahimi et al., 2013; Brandl et al., 2012)

Here are three typical features that are essential to battery management system: (1) State of Charge (SoC) is a percentage value that is generally used as a metric to quantify the amount of energy left in a battery compared with the energy it had when it was originally full. When SoC equals to 100%, it means the battery is now fully charged; and 0% SoC represents an empty battery. And SoC also indicates that how long a battery will continue to perform before it needs recharging. (2) State of Power (SoP) is the ratio of peak power to nominal power. The peak power is the maximum power that a battery can persistently provide for T seconds under the designed current, voltage, SoC and other power constraints (Shun et al., 2018). (3) State of

5

Health (SOH) is defined as the level of degradation of the battery due to the aging phenomena. (Remmlinger et al., 2011)

This thesis mainly focuses on the estimation of battery SoC, and compared the performances between different SoC estimation approaches. In the first Chapter of this work, the history and prospects of electric vehicles and the motivation of this project are introduced. Five categories of typically SoC estimation techniques including open-circuit voltage (OCV) mapping, coulomb-counting, model-based observers, data-driven methods and impedance-based methods, as well as their pros and cons are discussed in Chapter 2. In Chapter 3, the structure and principles of the testbench are explained. The testing procedure and experimental results using coulomb-counting, OCV mapping and machine learning model-based method captured by real-time battery testing system are summarized in Chapter 4.

Chapter 2: SoC Estimation Techniques

SoC is defined as the currently available capacity in a battery divided by its nominal capacity. An accurate SoC estimation plays a critical role in a reliable battery management system. Unlike the fuel level in traditional combustion engine vehicles, the SoC cannot be directly measured in EV applications. However, SoC is internally linked with direct measurement (voltage, current, temperature and capacity) and can be extracted by using battery intrinsic relations or control theory. (Lee et al., 2008; Pang et al., 2001; Piller et al., 2001) Five typical methods have been proposed to estimate the SoC in lithium-ion batteries in this chapter.

2.1 Open Circuit Voltage (OCV) Mapping

Open circuit voltage (OCV) is a parameter that projects the changes in electric energy of lithium-ion batteries. It can be used to estimate battery SoC, as well as manage the battery pack. The most straightforward method to estimate SoC is mapping the OCV to SoC, as a one-to-one translation can be found between SoC and OCV under certain conditions. The translation is a nonlinear monotone relationship and ought to be general enough for representing different types of Lithium-ion battery, even when battery aging and temperature change happen.

The OCV-SoC curve can be generated by slowly charging/discharging the battery via a high-precision cycler that can largely avoid the effect of internal resistance. The cycler is able to save the measurements (voltages, currents) during the test, from which OCV and SoC are extracted and plotted as the OCV-SoC curve for OCV mapping. For simple SoC calculation, a curve fitting is usually applied to convert the test data into some fitting data that could be expressed as a polynomial, then the SoC could be calculated with the polynomial model.

Given a specific OCV, the corresponding SoC can be accurately interpreted if the measured condition matches the one where the OCV-SoC map is acquired. In other words, the

OCV-SoC map varies with testing conditions, such as temperature and aging status, which introduce a significant amount of variability and can bias the SoC estimation (Chemali et al., 2016; Waag et al., 2014; Baronti et al., 2011). Different OCV-SoC curves at different temperatures are depicted in Fig. 4, the average error between each curve at 3.29V is 9%. OCV-SoC relation with aging effect is shown in Fig. 5, the largest error between the fresh cell and the aged cell is 7%.
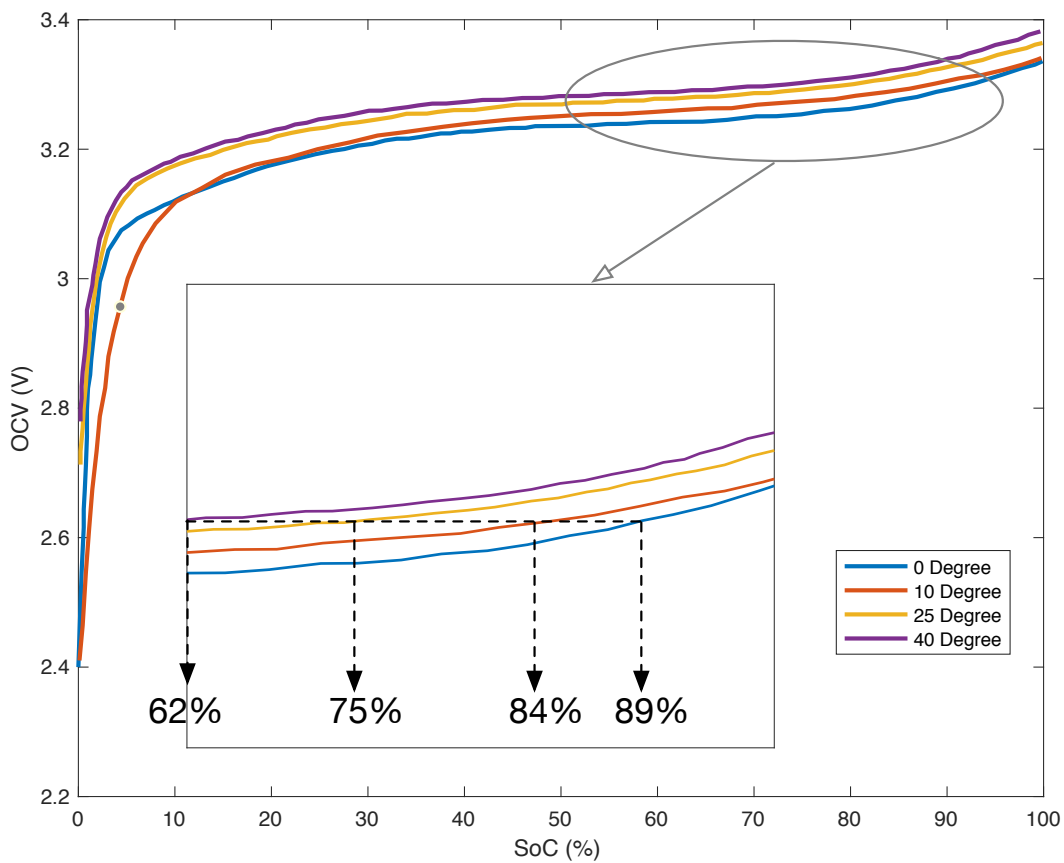
Figure 4: OCV-SoC Curve dependency of temperature.[3]

[3] Data from Elabadine et al. *A Novel Hybrid Technique to Predict the Lithium-Ion Battery's Behavior and Estimate the Intern Impedance.* International Journal of Emerging Electric Power Systems, Jul. 2017.
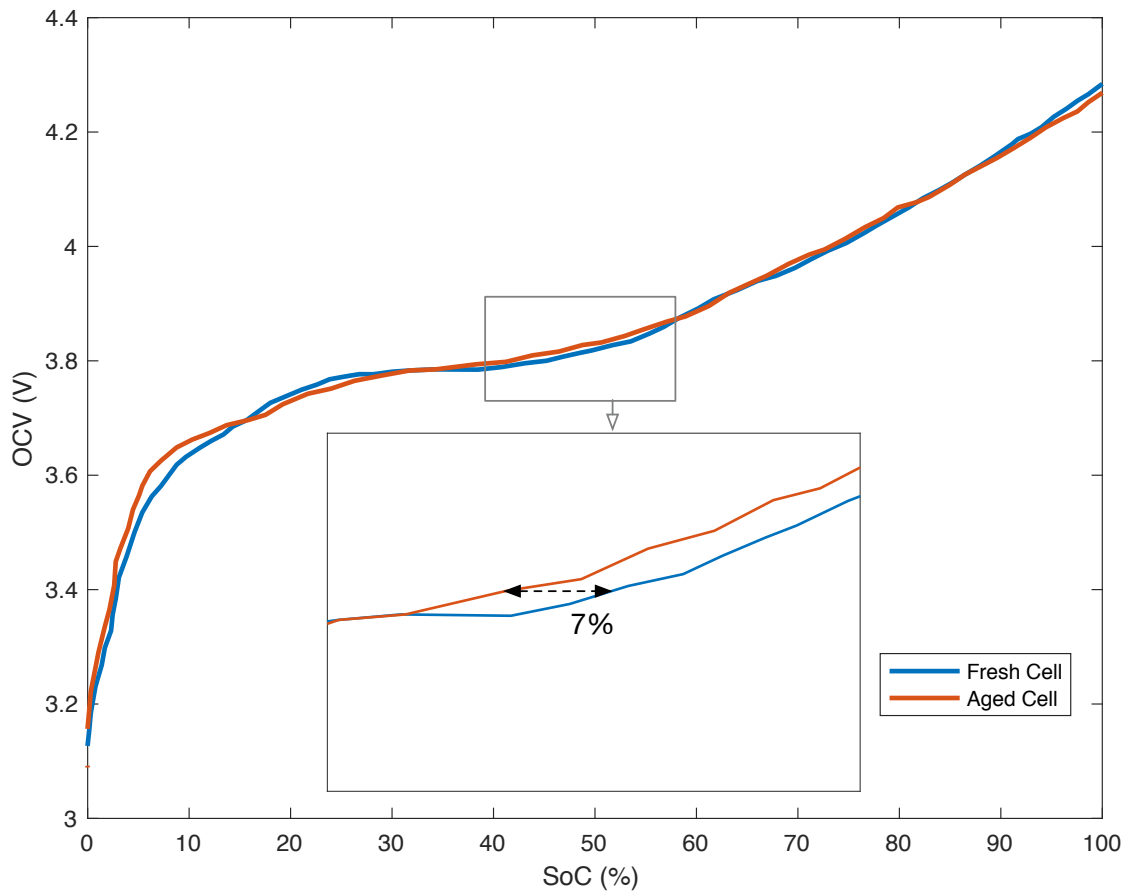
Figure 5: OCV-SoC Curve dependency of aging status.[4]

Even the direction of current flow (charging/discharging) will affect the OCV-SoC map significantly according to (Roscher et al., 2011). Fig. 6 showcases the different OCV-SoC curves when a same battery is under charging and discharging, respectively. If the OCV-SoC curve generated from discharge data is used for charging period OCV mapping, the largest error in this case is 13%, thus the SoC result would be no longer accurate.

---

[4] Data from Ovejas and Cuadras. *State of charge dependency of the overvoltage generated in commercial Li-ion cells*. Journal of Power Sources. 418. pp.176-185, 2019.
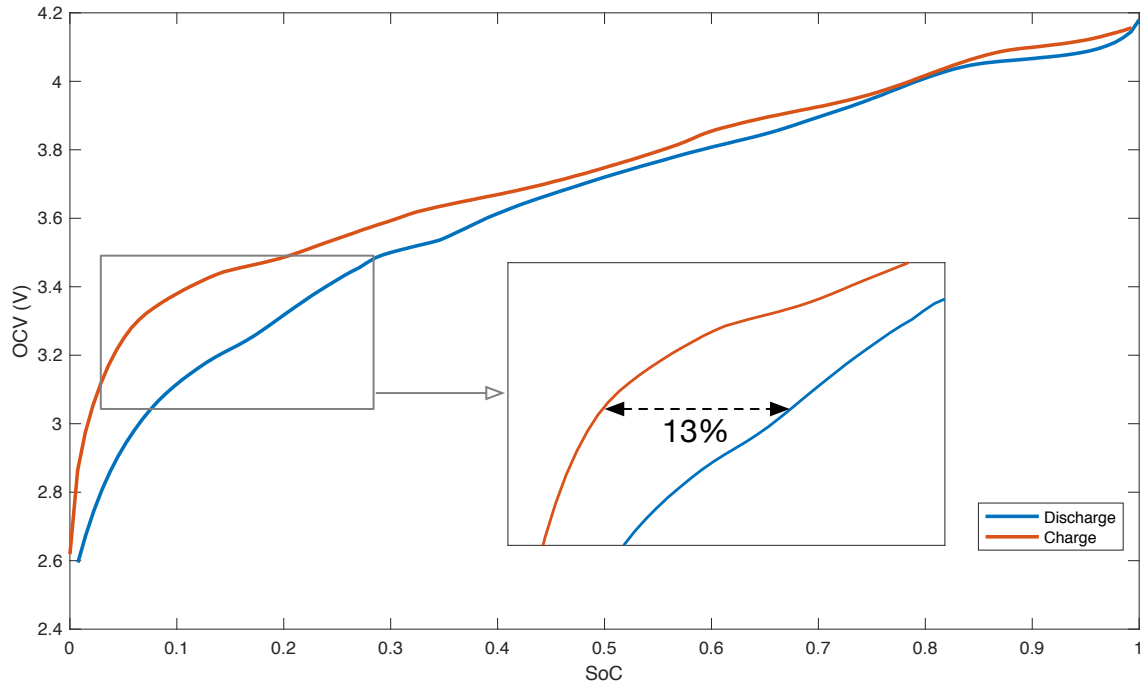
Figure 6: Different OCV-SoC Curves when charging and discharging.

In addition, complete electrochemical equilibrium cannot be achieved within a short time frame (Waag et al., 2013). Therefore, while the battery is under load, it is unfeasible to perform real-time updates of SoC based on OCV measurements. For these reasons, OCV-based SoC estimation is commonly used as a complementary or corrective method running in the background (Xiong et al., 2017).

2.2 Coulomb-Counting

Coulomb-Counting is one of the simplest approaches to calculate the SoC value. It identifies a SoC estimation technique that integrates the battery current, i.e. counts the Coulombs. Hence, it can identify an SoC difference after requiring knowledge of an initial SoC value, which can be obtained with an OCV-SoC map in a well-known condition. Coulomb-counting (or Ah counting) integrates the current passed in/out of the battery with respect to time and converts it to the SoC using the following expression:

$$SoC = SoC_0 + \eta \int \frac{i}{C} dt \qquad (1)$$

where SoC_0 is the initial state of SoC; C is the present capacity of the cell. The

charging/discharging efficiency is denoted as η. The current that charges/discharges the battery

is i. However, the accuracy of SoC estimation would be compromised if low-res current sensors

are used or the capacity is not updated as the battery ages (Baronti et al., 2011; Ng et al., 2009;

Baccouche et al., 2018) as can be seen in Fig. 7. The error in this figure is exaggerated for

descriptive purpose. A 0.5A bias in current sensor will be accumulated to a 0.17% SoC

estimation error in 1hr. Particularly, in situations where the SoC cannot be regularly corrected by

OCV-based methods, the predicted SoC significantly drifts away from the true value and

misleads other functions in battery management system. As a result, coulomb-counting is

commonly used in the laboratory environment, where the aforementioned uncertainties can be

reasonably controlled.

An improved coulomb-counting technique combined coulomb-counting with a

periodically OCV correction can also be used in order to control those uncertainties, it is able to

eliminate the accumulated errors that caused by low-res current sensors. Instead of using

coulomb-counting to estimate the SoC in the whole driving process, SoC corrections will be

implemented at periodically time stamps. (i.e. for every 10% SoC drop). As is evident in Fig. 8,

the significantly drift-away coulomb-counting shown in Fig. 7 is corrected for each 10% SoC,

the further error accumulation therefore is eliminated. Here, the SoC correction is acquired from

voltage measurements, based on the battery OCV-SoC curve.
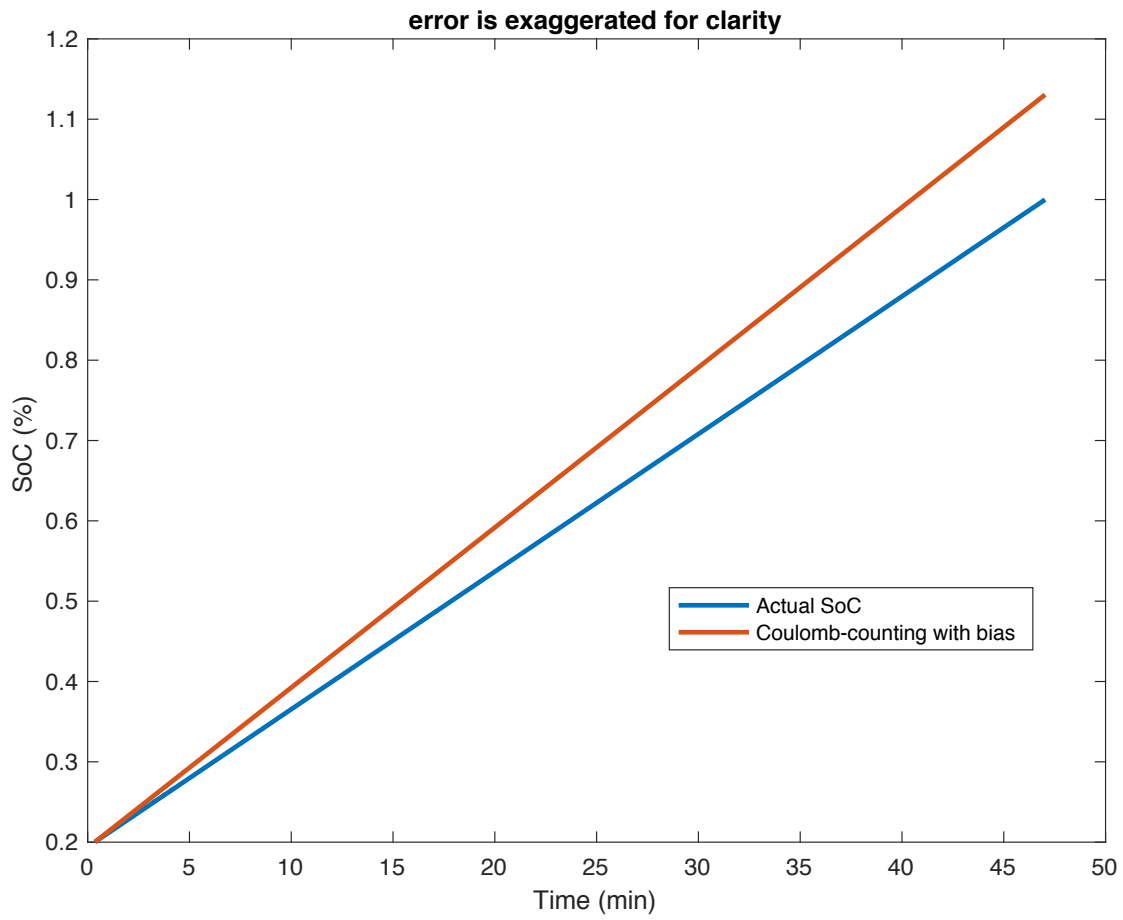
Figure 7: Coulomb-counting with current sensor bias.
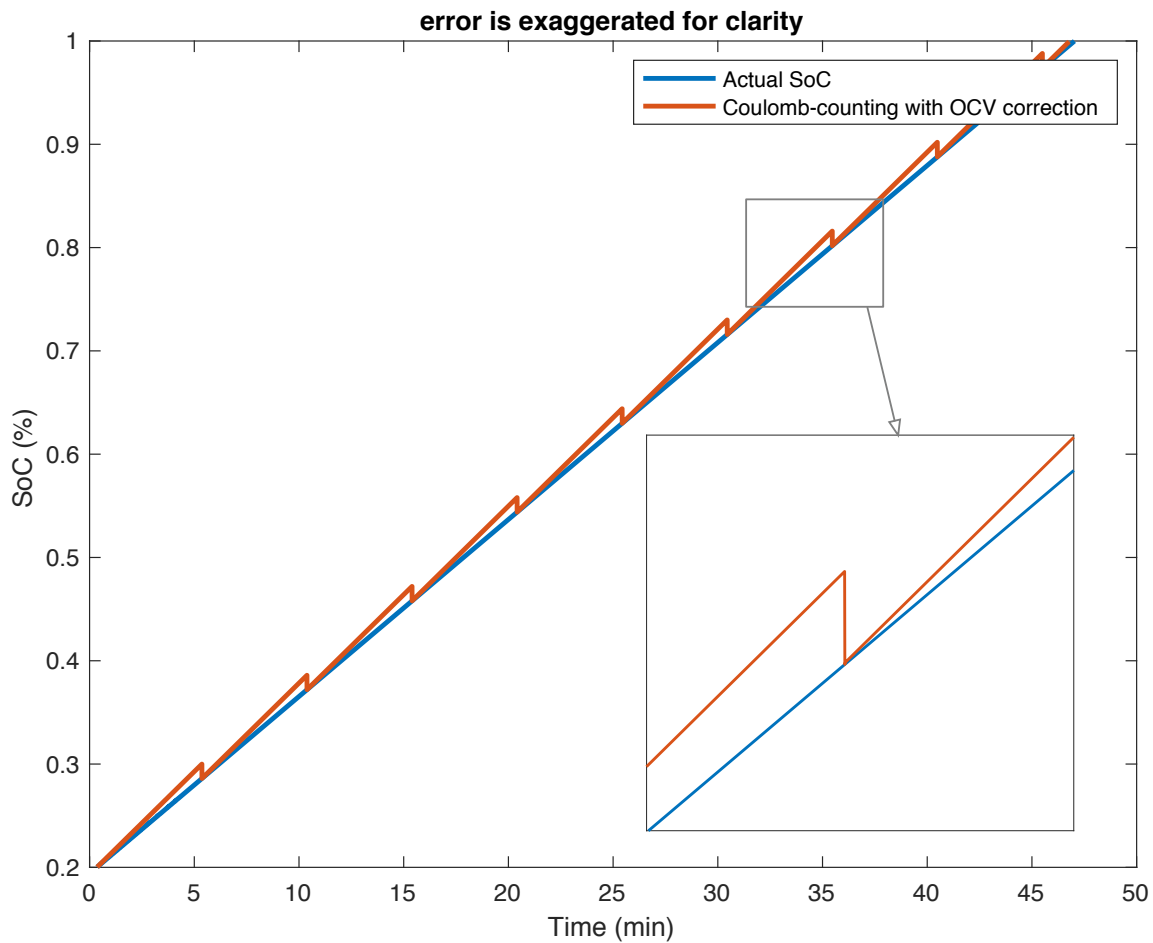
Figure 8: Improved Coulomb-counting to avoid the estimated SoC drift away.

2.3 Model-based Observer

To reduce the uncertainties of the open-loop SoC estimation methods mentioned previously, techniques with feedback mechanisms to correct possible bias and real-world compromises (such as sensor resolution) have been extensively investigated. Adapted filters and observers are commonly adopted, combined with an electric circuit model (ECM) or an electrochemical model. (Lai et al., 2018) Particularly, Kalman-Filter (KF) based technologies has been heavily researched as they provide reasonable estimation accuracy and relatively robust performance (Arasaratnam and Haykin, 2009; Afshari et al., 2015; Habibi, 2007; Domenico et

al., 2008; Ahmed et al., 2014; Speltino et al., 2009; Welch and Bishop, 1995; Hua et al., 2012; He et al., 2013; Li et al., 2013).

Kalman-Filter (KF) utilizes linear state-space model, as illustrated in Fig. 9, and implements initialization and computation for time update and measurement update, the equations of the Kalman filter are summarized as follow:

state equation:

$$x_{k+1} = A_k x_k + B_k u_k + w_k \tag{2}$$

observation equation:

$$y_k = C_k x_k + D_k u_k + v_k \tag{3}$$

Initialization:

$$\hat{x}_0^+ = \mathbb{E}[x_0] \tag{4}$$

$$\sum_{\tilde{x},0}^+ = \mathbb{E}[(x_0 - \hat{x}_0^+)(x_0 - \hat{x}_0^+)^T] \tag{5}$$

State estimate time update:

$$\hat{x}_k^- = A_{k-1}\hat{x}_{k-1}^+ + B_{k-1}u_{k-1} \tag{6}$$

Error covariance time update:

$$\sum_{\tilde{x},k}^- = A_{k-1} \sum_{\tilde{x},k-1}^+ A_{k-1}^T + \mathbb{E}[w_k w_k^T] \tag{7}$$

Kalman gain matrix:

$$L_k = \sum_{\tilde{x},k}^- C_k^T [C_k \sum_{\tilde{x},k}^- C_k^T + \mathbb{E}[v_k v_k^T]]^{-1} \tag{8}$$

State estimate measurement update:

$$\hat{x}_k^+ = \hat{x}_k^- + L_k[y_k - C_k\hat{x}_k^- - D_k u_k] \tag{9}$$

Error covariance time update:

$$\sum_{\tilde{x},k}^{+} = (I - L_k C_k)\, \mathbb{E}[\tilde{x}_k \tilde{x}_k^T]^{-} \tag{10}$$

where $x_k \in \mathbb{R}^n$ is the state vector at time k, the minimum mean squared error estimate of the true state x_k is denoted as $\hat{x}_k$, $\tilde{x}_k$ is the state estimator error that defined as x_k minus $\hat{x}_k$, $u_k \in \mathbb{R}^p$ is a known system input. The vectors $w_k \in \mathbb{R}^n$ and $v_k \in \mathbb{R}^m$ describe independent, zero-mean, Gaussian noises that model some unmeasured input which affects state and output of the system, respectively. The system output is $y_k \in \mathbb{R}^m$. The matrices $A_k \in \mathbb{R}^{n \times n}$, $B_k \in \mathbb{R}^{n \times p}$, $C_k \in \mathbb{R}^{m \times n}$ and $D_k \in \mathbb{R}^{m \times p}$ represent the dynamics in the system.
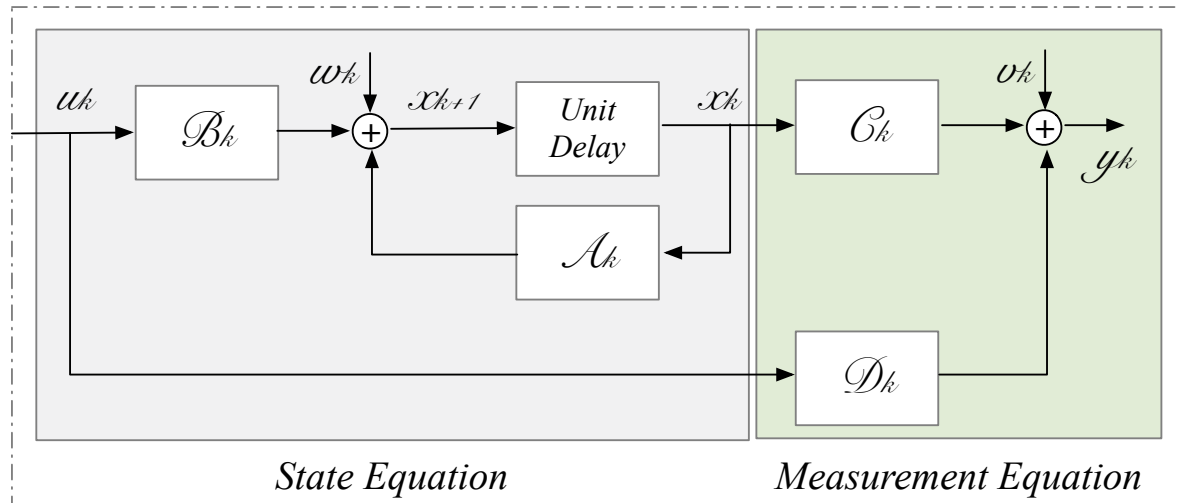
Figure 9: Diagram of linear discrete-time system in state-space form.

The Kalman filter provides a theoretically elegant and time-proven method to filter measurements of system input and output to produce an intelligent estimate of a dynamic system's state. The equations involve basic matrix operations that are easy to implement on digital-signal-processing (DSP) chips. A side effect of the Kalman filter is that the state uncertainty matrix is automatically produced, giving an indication of the error bound on the estimate.

The Kalman Filter is the optimum state estimator for linear systems, when the system is nonlinear, a linearization process is applied on the nonlinear system with a linear time varying system (LTV). A nonlinear system block diagram is illustrated in Fig. 10. If the KF is employed on this linear time varying system, it means an Extended Kalman Filter (EKF) is used for this nonlinear system (Han et al., 2009; He et al., 2011; Kim and Cho, 2011; Plett, 2004; Rubagotti et al., 2009; Taborelli and Onori, 2014; Vasebi et al., 2007). The EKF generally works pretty well even if itself is not optimal. The functions of EKF are listed below:

Nonlinear space model:

$$x_{k+1} = f(x_k, u_k) + w_k \tag{11}$$

$$y_k = g(x_k, u_k) + v_k \tag{12}$$

Initialization:

$$\hat{x}_0^+ = \mathbb{E}[x_0] \tag{13}$$

$$\sum_{\tilde{x},0}^+ = \mathbb{E}[(x_0 - \hat{x}_0^+)(x_0 - \hat{x}_0^+)^T] \tag{14}$$

Definition:

$$\hat{A}_k = \left.\frac{\partial f(x_k, u_k)}{\partial x_k}\right|_{x_k = \hat{x}_k^+} \tag{15}$$

$$\hat{C}_k = \left.\frac{\partial g(x_k, u_k)}{\partial x_k}\right|_{x_k = \hat{x}_k^-} \tag{16}$$

State estimate time update:

$$\hat{x}_k^- = f(\hat{x}_{k-1}^+, u_{k-1}) \tag{17}$$

Error covariance time update:

$$\sum_{\tilde{x},k}^- = \hat{A}_{k-1} \sum_{\tilde{x},k-1}^+ \hat{A}_{k-1}^T + \mathbb{E}[w_k w_k^T] \tag{18}$$

Kalman gain matrix:

$$L_k = \sum_{\tilde{x},k}^{-} \hat{C}_k^T [\hat{C}_k \sum_{\tilde{x},k}^{-} \hat{C}_k^T + \mathbb{E}[v_k v_k^T]]^{-1} \tag{19}$$

State estimate measurement update:

$$\hat{x}_k^+ = \hat{x}_k^- + L_k[y_k - g(\hat{x}_k^-, u_k)] \tag{20}$$

Error covariance time update:

$$\sum_{\tilde{x},k}^{+} = (I - L_k \hat{C}_k) \, \mathbb{E}[\tilde{x}_k \tilde{x}_k^T]^- \tag{21}$$

where $f(x_k, u_k)$ is a nonlinear state transition function and $g(x_k, u_k)$ is a nonlinear measurement function.
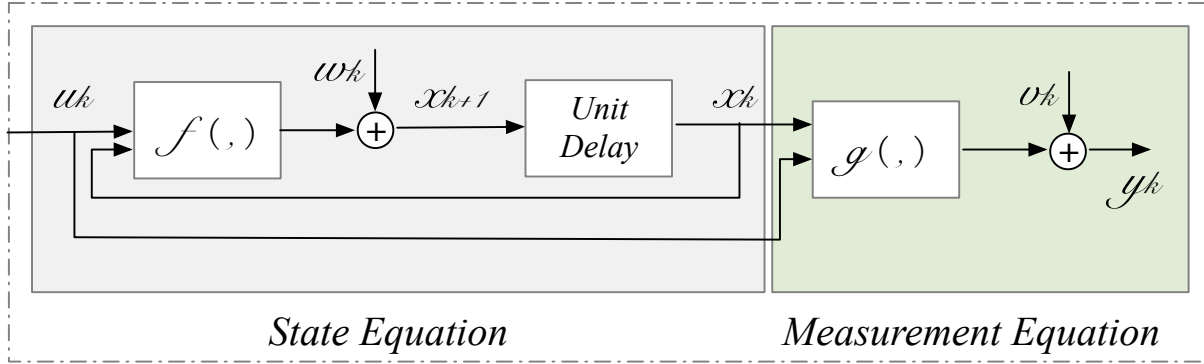
Figure 10: Diagram of nonlinear discrete-time system in state-space form.

Apart from KF, the particle filter and adaptive observer are applied to further improve the SoC estimation accuracy (He et al., 2012; Rubio et al., 2014; Zheng et al., 2014; Ning et al., 2016).

However, constructing such an observer requires precise system modeling for the specific type of battery in the system and repetitive hand tuning to select a well-behaved covariance matrix (He et al., 2012). Parameters of the particular battery and accuracy of the selected model are variables that are closely concerned with the estimation result. As the battery ages, the derived battery model using a 'fresher' cell's data is biased and may even be invalid. The capacity decreases while impedance increases for aged cells, which can result in an offset/error

from the true SoC and even divergence of the observer. In addition, the initial states of the observer that are fed from external sources significantly affect the performance of the estimator, in terms of convergence and accuracy.

2.4 Data-driven Methods

With advancements in computation and an abundance of real-world data, machine learning or specifically neural network-based methods are providing researchers with the ability to achieve significant advancements in many fields (Krizhevsky et al., 2012; CireAn et al., 2012; Hinton et al., 2012; Ma et al., 2015; Wang et al., 2016). Machine learning techniques, such as fuzzy logic, support vector machines (SVMs) and neural networks are used to analyze the nonlinear relationship between observable variables and battery states (Li et al., 2011; Alvarez et al., 2013; Hu et al., 2014; Eddahech et al., 2012; Guo et al., 2017; Dong and Wang, 2014; Tong et al., 2016; Hannan et al., 2018). Fuzzy logic was used to define battery working state (BWS) to solve the battery over-discharge problem and associated damage resulting from inaccurate SoC estimation. LiB state estimation based on SVMs and optimized support vector machines for regression (SVRs) are utilized for EV applications under diverse driving conditions. Especially, SoC estimation applying neural network-based methods has drawn attention, the working principle of which shown in Fig. 11.
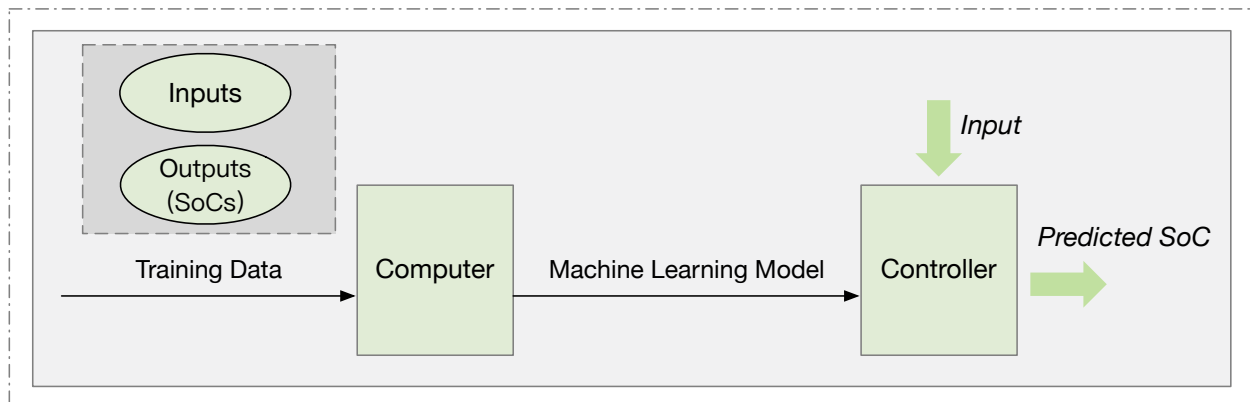
Figure 11: Working principle of data-driven methods.

Compared to a 2% average SoC error achieved by model-based observers (Plett, 2004; Xiong et al., 2017), 4% RMS error on terminal voltage is achieved with 2-layer neural network and 30 neurons in the hidden layer (Charkhgard and Farrokhi, 2010). However, should further error reduction be desired, neural networks need the help of external filtering/observer (like Kalman-filter in Du et al. (2014). Chemali, Kollmeyer, Preindl, et al. directly mapped the measurements of the cell (instantaneous and average terminal voltage, temperature, and average current) to the SOC estimation and is able to achieve a mean absolute error below 1% in Chemali et al. (2018).

Despite many studies on data-driven SoC estimation successfully achieved excellent results, there are problems remain unsolved (Li et al., 2019). For instance, the output of FNN-based approach only depends on current input, whereas the current SoC is also associated with history observable variables, which makes it difficult for FNN to process time-sequence problems.

2.5 Impedance-based Methods

The dependency between impedance of battery and SoC is utilized in researches on the SoC estimation for Lead acid, NiMH, nickel-cadmium and LiBs. The SoC has been extensively investigated as a function of impedance variation (Elabadine et al., 2017; Cuadras and Kanoun, 2009; Zenati et al., 2010; Waag et al., 2013; Ovejas and Cuadras, 2018). However, the impedance changes significantly with the battery's aging status, as shown in Fig. 12. The impedance-based method is no longer a good indicator of SoC as the battery ages. Additionally, the sensitivity of impedance on SoC is much lower than on temperature, as a result, a very accurate impedance-based method often requires compensation from the temperature. However,

such accuracy cannot always be maintained for batteries in BEVs or HEVs, due to the rapid

temperature change in driving process.
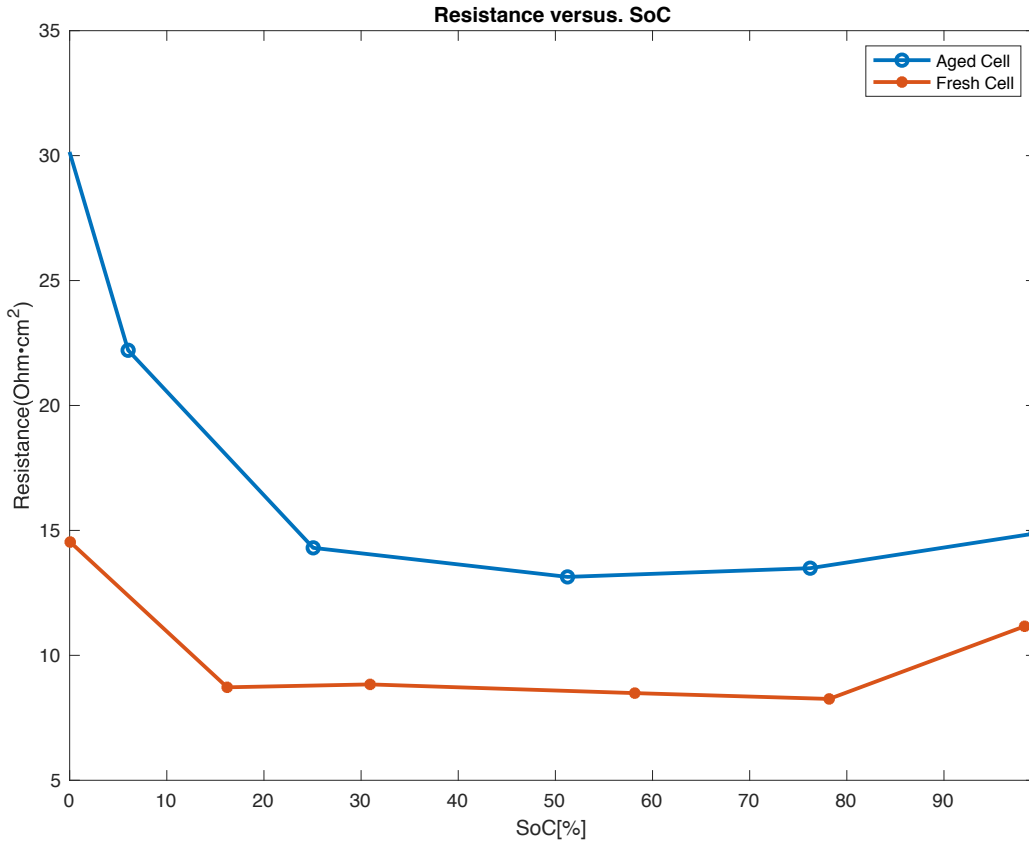
Figure 12: Impedance characteristic at different aging status.[5]

[5] Data from Ovejas and Cuadras. *Impedance Characterization of an LCO-NMC/Graphite Cell: Ohmic Conduction, SEI Transport and Charge-Transfer Phenomenon.* Batteries 2018, 4(3), 43, 2018.

Chapter 3: System Set-up

The goal of this project is to compare the results of several SoC estimation techniques, like aforementioned OCV Mapping, Coulomb-counting, and a newly developed method applying machine learning model that promises both rapid response and high accuracy. The flowchart of the project design is demonstrated in Fig. 13.
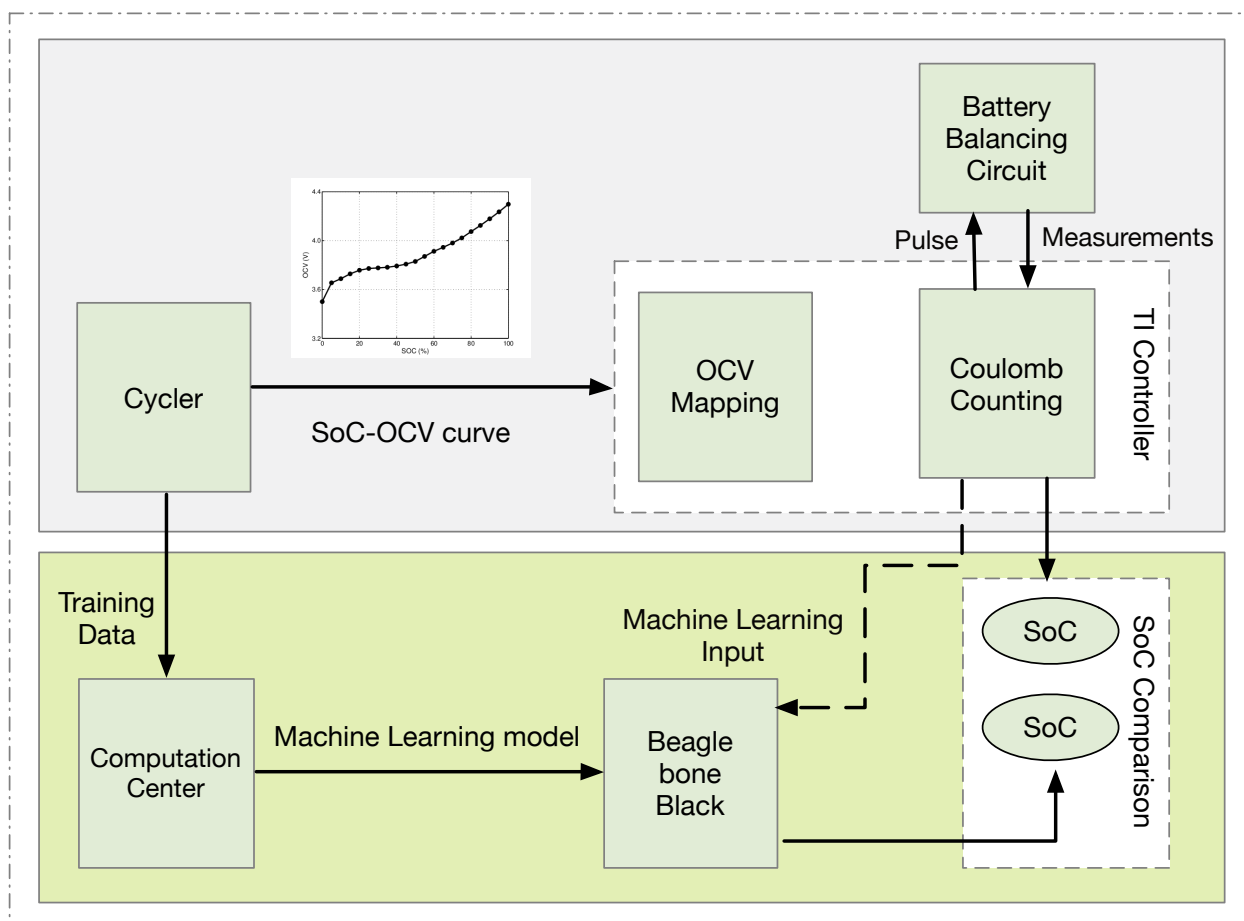
Figure 13: Flowchart of the project.

This thesis hypothesizes that passing current pulses through a battery and measuring the voltage response to these pulses can be used to retrieve information about a lithium-ion battery's SoC. Since these measured electrochemical responses do not have an obvious relationship with the SoC, a neural-network can be used to learn the relationship and reconstruct the information.

The injected pulses are therefore expected to help decrease the error of SoC estimation to some extent.

3.1 Test by the Cycler

The high-precision cycler, shown in Fig. 14 is used to charge and discharge the battery in a slow rate, i.e. 0.1 C-rate, to avoid the influence from internal resistance and acquire the true capacity. The smaller the current rate is, the better the internal resistance can be ignored (Wang, 2016). The real-time battery cycler is capable of testing the cells using constant current (CC), constant voltage (CV), CCCV, and dynamic current profiles (driving cycles) with a sampling resolution of 0.1s. The hi-res measurements, including voltage, current and temperature, are uploaded to the database for generating OCV-SoC curves as the basis for OCV Mapping and training of machine learning model.

Figure 14: Photo of the cycler.

During the tests with cycler, the capacity should be checked regularly in order to interpret the SoC correctly. Since the cpacity will fade if the battery ages, which significantly degrade the

performance of SoC estimation as it highly rely on the present capacity according to the SoC definition in Eq. (1).

A higher current level contributes to lower estimation error (Wang et al., 2019), as depicted in Fig. 15. However, the feasibility of the current amplitude in the real battery system needs to be investigated. As for selecting the amplitude of the current pulses, a trade-off was made between estimation accuracy and feasibility. As a result, the current amplitude is chosen to be 1 C-rate since it potentially will decrease the error more while keeping the cells away from maximum allowed current. Fig. 16 shows the plot of the 3-minutes pulse current consists of A 1-min long charge pulse and discharge pulse with 1-min rest between them. Note that in this thesis the sign convention for the current is negative for charging and positive for discharging.
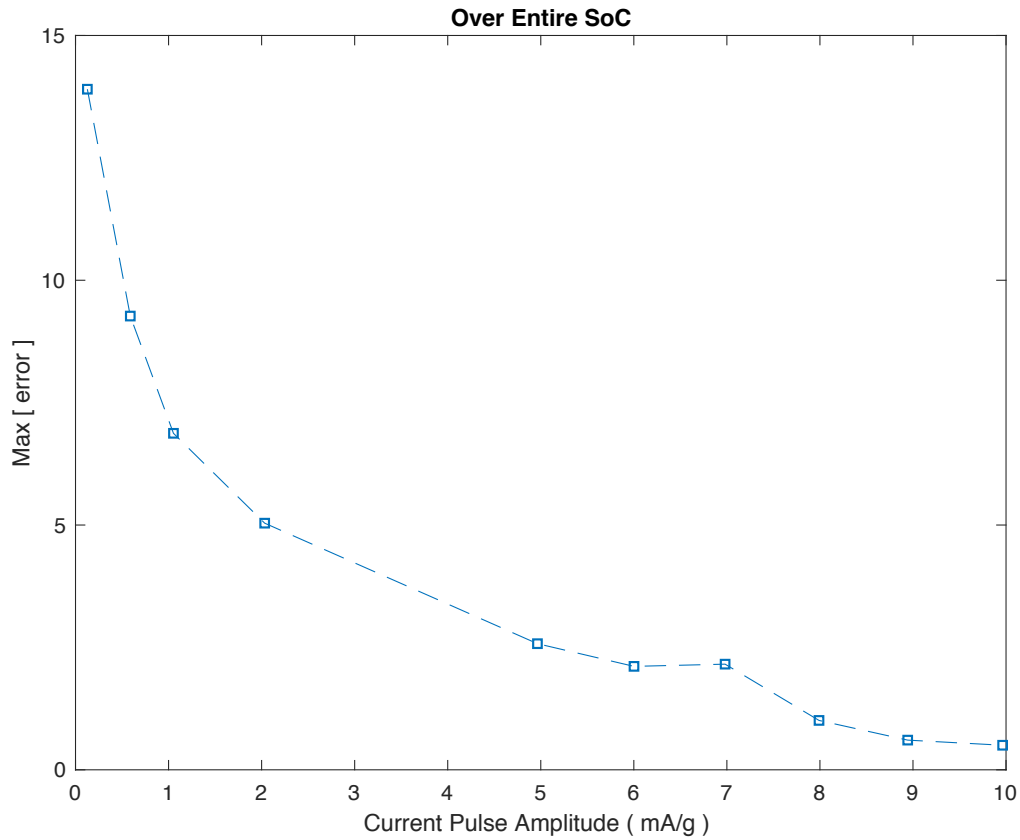
Figure 15: Error of SoC estimation at different current pulse amplitude.[6]
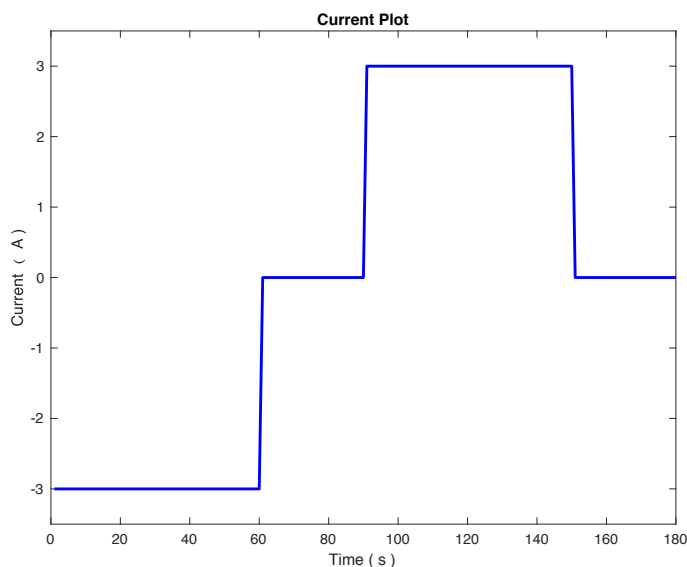
Figure 16: 1 C-rate pulse current plot.

Aging a battery is a time-consuming task. To accelerate the aging process, a pre-defined aging procedure is proposed here. The cells under test fully discharge with a CC at 1 C-rate, and followed by fully charge with a CC at 1 C-rate to maximum voltage and CV until current drops below 150 mA. The aging test will be terminated when the capacity reaches 80% of its original one, which is normally called end-of-life (EOL) for EV application.

The systematic testing procedure composed of capacity check, pulse train and aging test is proposed in Fig. 17.

---

[6] Data from Wang et al. *High-Fidelity State-of-Charge Estimation of Li-Ion Batteries using Machine Learning*. 2019.
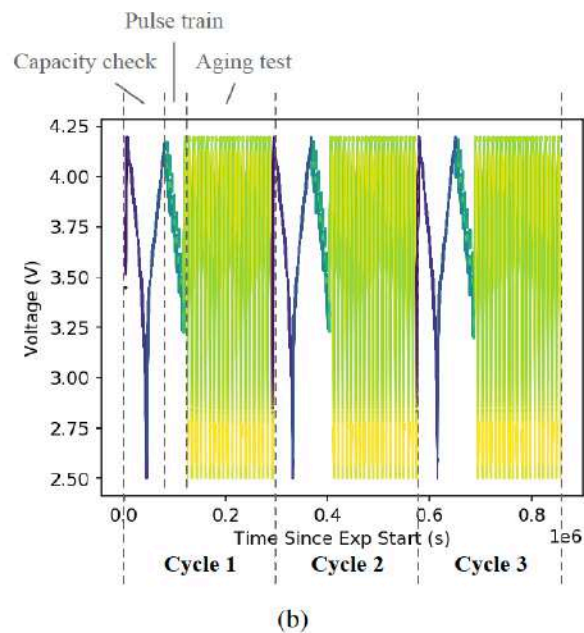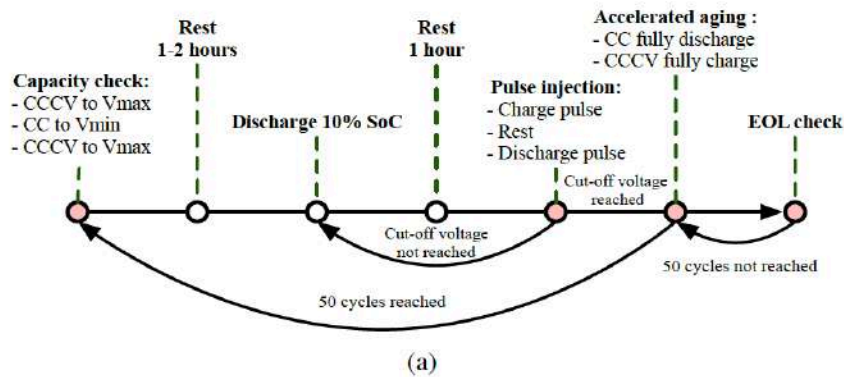
Figure 17: Entire testing procedure by battery cycler: (a) the Flowchart, (b) Complete test sequence captured by the cycler.[7]

3.2 Testbench Intro

The test bench employed in this thesis is a three-layer structure system, including a

battery balancing circuit, a TI controller and a higher-level controller, as shown in Fig. 18.

---

[7] Figure from Wang et al. *High-Fidelity State-of-Charge Estimation of Li-Ion Batteries using Machine Learning*. 2019.

Figure 19 showcases the zoomed-in photo of the batteries used in real-world experiments, which are Lithium-ion rechargeable cells by Samsung SDI, and the parameters, including nominal capacity, nominal voltage, charging voltage and discharge cut-off voltage, are specified in Table 1.
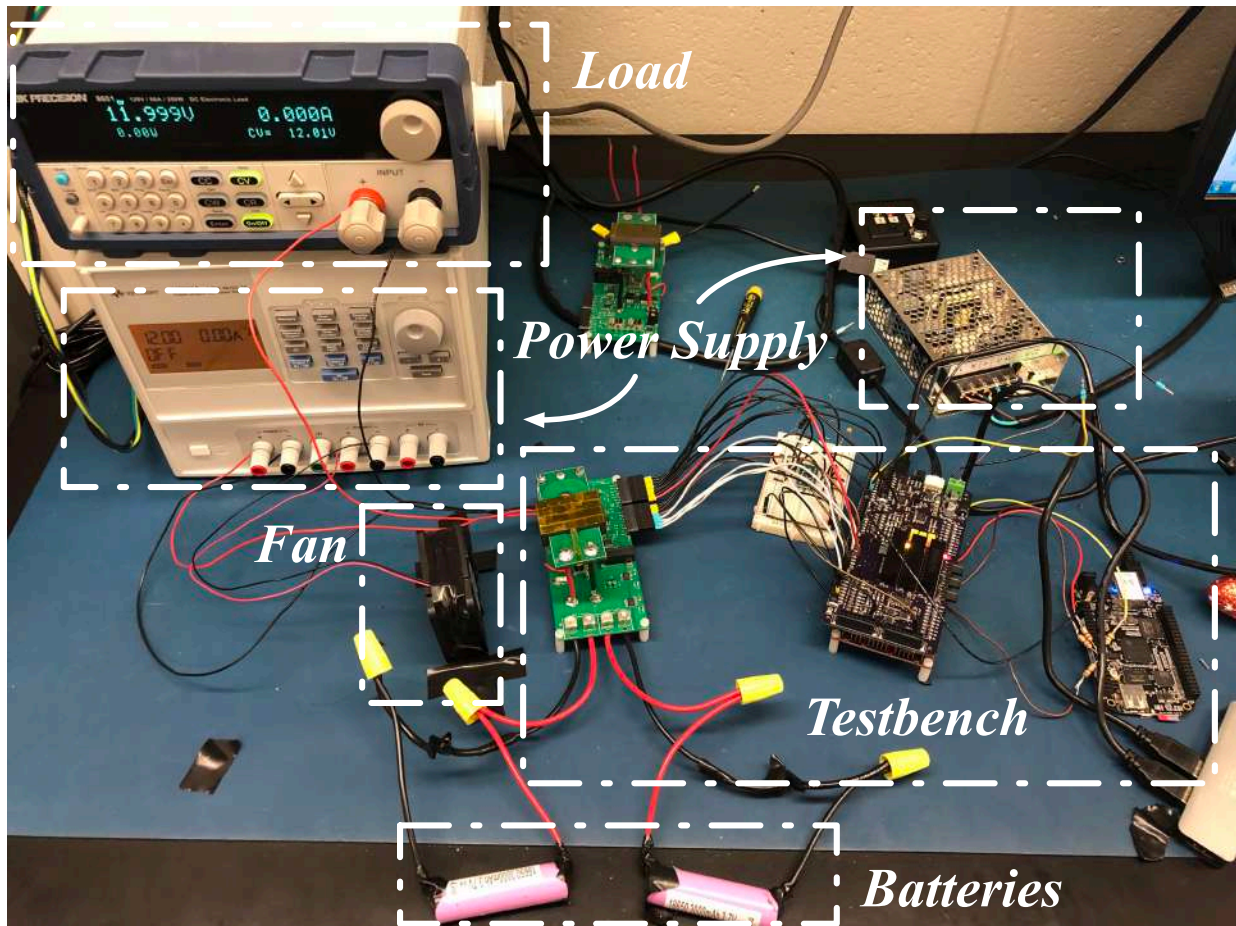
Figure 18: Photo of the real-world testbench.
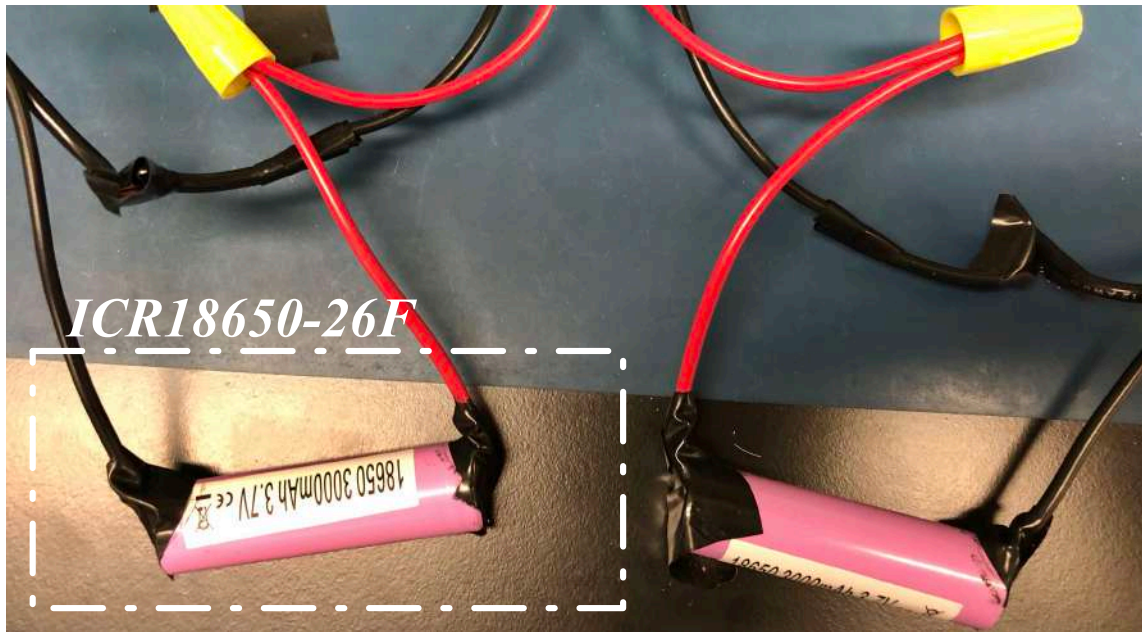
Figure 19: Photo of the Lithium-ion rechargeable batteries.

3.2.1 Battery Balancing Circuit

Normally, when the batteries are connected in series, there is somewhat difference in battery capacity or SoC for individual cells under load conditions, which is not desired in most cases as this means the charge/discharge for the whole battery pack has to be stopped as one of it reaches over charging/discharging protection. Therefore, a battery balancing circuit, which is able to accommodate those SoC differences between battery cells by transferring energy from or to individual cells, is in demand in order to monitor and regulate the behaviors of batteries (Wang and Preindl, 2019).

Fig. 20 is the topology of the employed half-full bridge circuit that is able to achieve battery balancing, which is divided into four parts. The high voltage side, also the input of this circuit, includes two battery cells. The half bridge on the primary side allows the two cells to be balanced by one converter. It is designed to convert the DC that from the battery side to AC as the battery can only generate DC power, while the transformer requires AC input. The full bridge

circuit on the secondary side then works as a rectifier to implement the conversion from AC to DC, which offers a more stable and reliable voltage to low voltage side. Additionally, the transformer in this topology is used for bidirectional power transmission and galvanic isolation, hence, the input batteries can either be charged or discharged by controlling direction of their power separately. If the two battery cells are at different SoC levels, in order to realize the battery balancing function, the currents of two cells are adjusted independently by controlling the input power and the cell-to-cell current. A balanced state will be reached by charging the low-SoC cell and discharge the high-SoC cell, until both cells have achieved an identical SoC value.
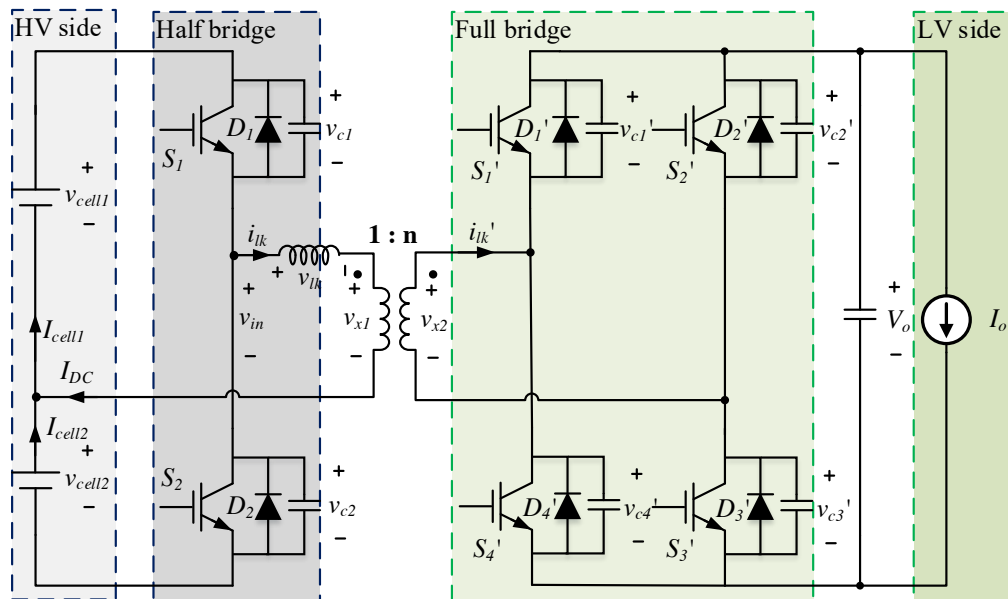
Figure 20: Topology of the battery balancing circuit.[8]

The photo of this battery balancing circuit is shown below:

---

[8] Figure from Wang and Preindl. *Dual Cell Links for Battery-Balancing Auxiliary Power Modules: A Cost-Effective Increase of Accessible Pack Capacity*. In IEEE Transactions on Industry Applications, 2019.
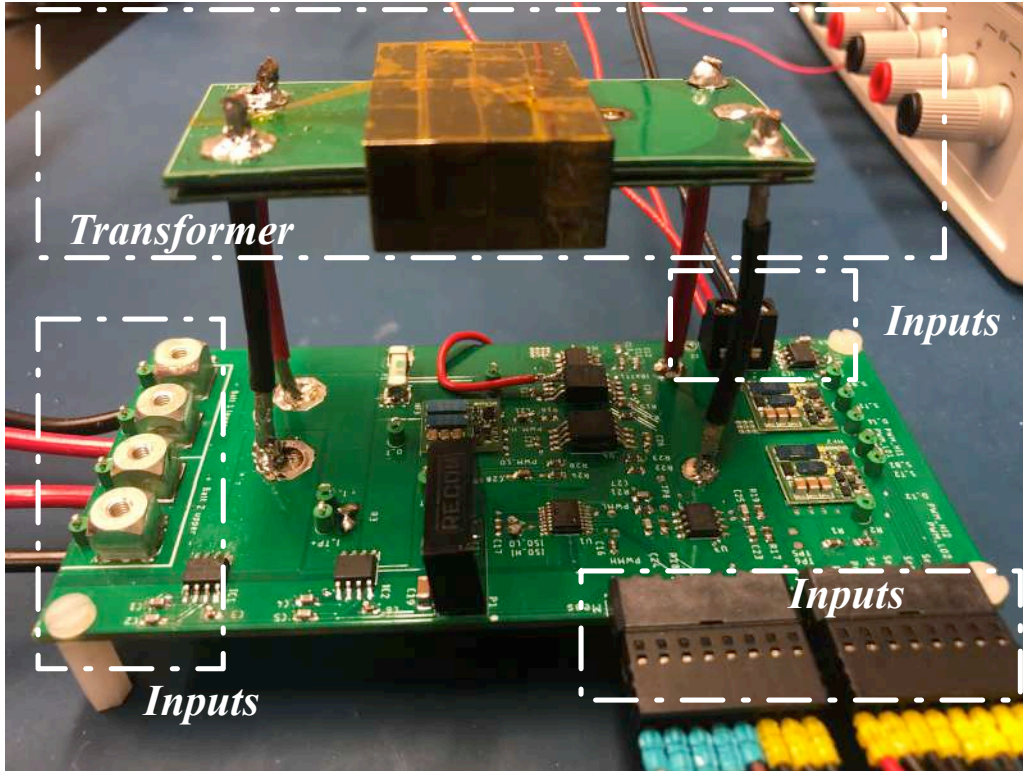
Figure 21: Photo of battery balancing circuit.

3.2.2 Lower-level Controller

The measurements of voltages and currents of two batteries from sensors in battery balancing circuit are sampled by the TI controller, which has two CPUs inside. CPU1 is mainly responsible for data processing and control strategies implementation in this controller, including averaging the instantaneous measurements, computing the SoC through calculating the coulombs, as well as maintaining constant current control. For CPU2, it basically sends the measurements (currents, voltages and SoCs) that saved in the shared memory of two CPUs to the higher-level controller. Fig. 22 is the photo of 28379D controller, along with an upper layer board that contains filtering modules and PWM level shifter.
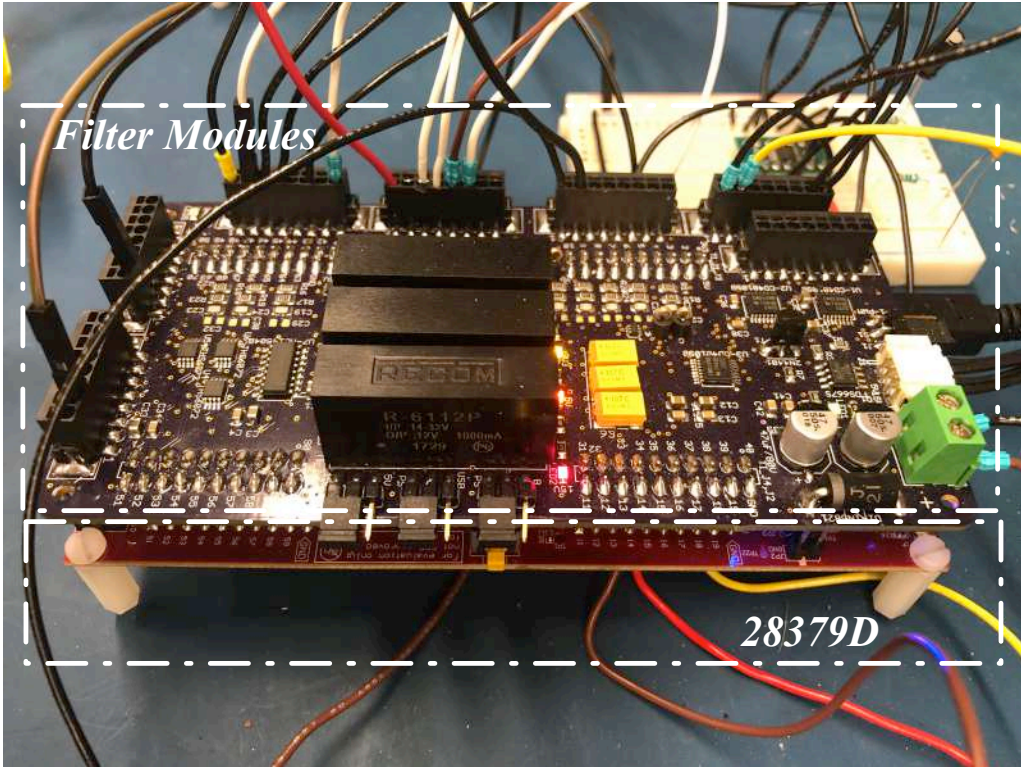
Figure 22: Photo of TI controller.

The control strategies inside the TI controller shown in Fig. 23 so as to realize constant current condition as experiments require. The input power and the cell-to-cell current are controlled by two closed control loops in the figure.
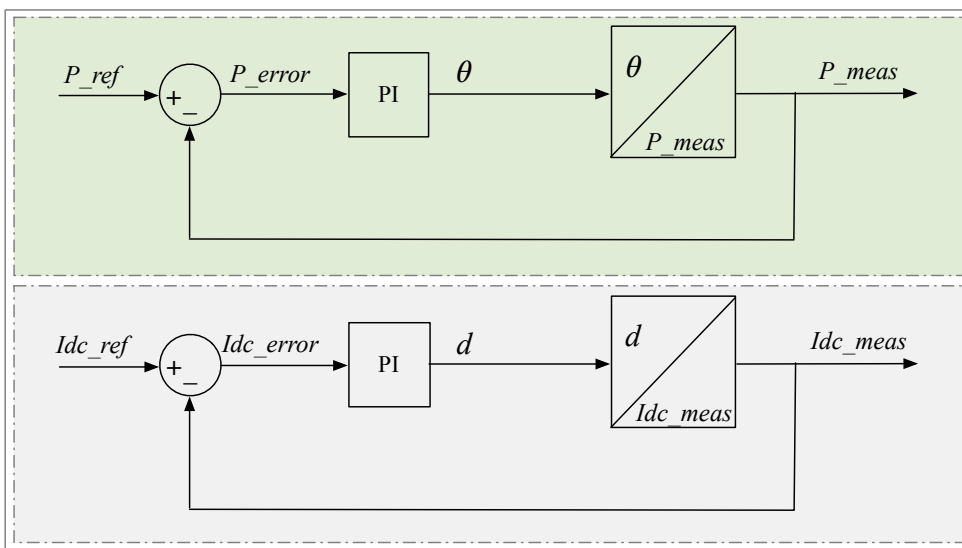
Figure 23: Control strategies in the microcontroller.

30

The upper closed loop control strategy applies a variable, phase shift, to control the input power. The control logic equations are given by:

$$P_{\_ref} = I_{cell1_{ref}} \times V_{cell1_{meas}} \times 2 \tag{22}$$

$$P_{\_meas} = I_{1_{meas}} \times V_{1_{meas}} + I_{2_{meas}} \times V_{2_{meas}} \tag{23}$$

where $P_{\_ref}$ is the reference input power of the sum of two cells, and I_{cell1_ref} is a command current value that describes the amplitude of the desired constant current. $P_{\_meas}$ is the real-time measurement of total input power that derived from instantaneous cell- currents and voltages; P_{error} is the difference between $P_{\_ref}$ and $P_{\_meas}$, which is fed into PI controller to generate a matching phase shift for the battery balancing circuit, the phase shift is denoted as θ.

Table 1: Controlling factors and parameters of the battery.

Kp1	Kp2	Ki2	Ki2
-0.001	-9.99e-05	-0.2	-0.7
Nominal Capacity	Maximum Charging/Discharging Current	Charging Voltage	Discharge Cut-off Voltage
3000mAh	4/15A	4.2 ± 0.05V	2.5V

This procedure is similarly adopted to obtain the other control strategy for the cell-to-cell current control by manipulating the difference of duty cycle between the two cells, as can be seen in the lower loop.

where I_{dc_ref} is the command value of the cell-to-cell current, the feedback of this closed loop control, I_{dc_meas}, is the cell-to-cell current that derived from instantaneous cell currents. I_{dc_error} depicts the result of I_{dc_ref} minus I_{dc_meas}, which is fed into PI controller to generate a corresponding duty cycle compensation, the duty cycle variable is denoted as d.

The constant current control at arbitrary current level can be achieved with the control logics described above, which is used in further SoC estimation experiments to let batteries be charged/discharged under a constant 1 C-rate current.

3.2.3 Higher-level controller (BeagleBone Black)

The higher-level controller in the testbench functions as a 'warehouse' for data storage and a 'computation center' for machine learning model as the insufficient storage space of TI controller. Data that handled by TI controller is transferred into the higher-level controller, BeagleBone Black, for data analysis and plotting via Serial Peripheral Interface (SPI) transmission (Leens, 2009; Saha et al., 2014). The SPI communication between controllers are sending measurements, such as cell average currents and voltages, the cell-to-cell current and SoCs, from the shared memory of CPU1 and CPU2 of the lower-level controller to the higher-level one in the format of 8-bit. Moreover, the matrices of machine learning model are saved in BeagleBone Black, and the computation that in order to get the output of the machine learning model is implemented in it as well. The photo of higher-level controller is shown in Fig. 24, the resistors in the figure are used to ensure reliable signal transmission.
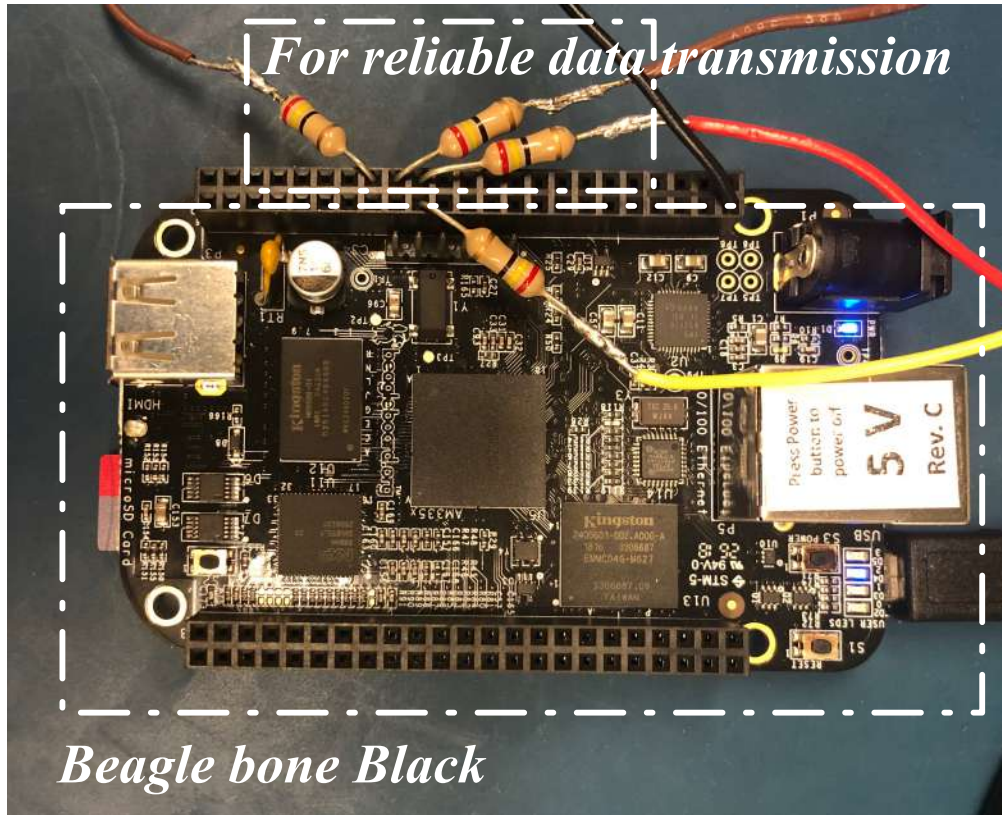
Figure 24: Photo of BeagleBone Black.

3.3 SoC Estimation in Real-Time System

The summarized diagram of the testbench is illustrated in Fig. 25. The entire system consists of (i) the peripheral hardware (the Battery balancing circuit); (ii) center and localized controllers that actuates the pulse injection, necessary BMS functions and circuit operation; and (iii) machine learning model stored in higher level controller (BeagleBone Black) that analyze the input data and generate the result for the SoC calculation; (iv) higher level controller that store the data from microcontroller for further analysis and plots.
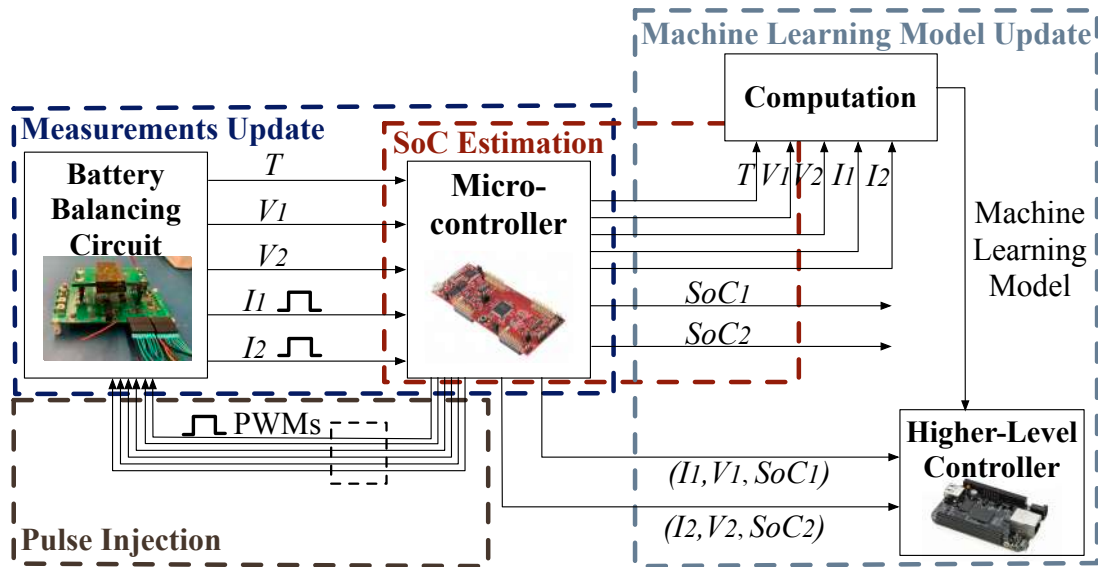
Figure 25: Diagram of the system.

3.3.1 Pulse Injection Module and Measurements Update Module

As the key novelty of the proposed concept, the pulses should be injected to the cells at the right timing with proper amplitude and duration as accurate as in laboratory environment.

The microcontroller is able to generate PWM pulses in the shape of given reference currents of the battery cells, with specified amplitude and duration of expected pulses, and pass them to battery balancing circuit to actuate the pulses into the battery cells. Additionally, the property (amplitude, period, etc.) of pulses could be arbitrarily adjusted by properly controlling the converters behavior.

All key features to estimate SoC are extracted with the measurements update module. The microcontroller equips high-resolution analog-to-digital converters that translates the analog signals (such as voltage/current measurements) to digital values, such that the computing unit can process them. The essential measurements (cell voltages, currents and temperatures) are captured and updated at the pre-defined sampling rate. Based on the sampling rate, the

measurements will be continuously uploaded to the computing unit via SPI protocol for further calculations of the machine learning model.

3.3.2 SoC Estimation Module

As explained previously in the flowchart, SoCs are calculated through coulomb-counting, OCV mapping and machine learning-based approach. Unlike OCV mapping method that has to wait for a long relax time in order to obtain the open-circuit voltage, which is not practical for real-world EV applications, the machine learning-based method yields both promptly response and high accuracy.

As the current pulses are injected to the cells through pulse injection module, the corresponding responses from battery cells are recorded by measurement update module to be used as inputs for the SoC estimation using machine learning model. The SoC estimation can be performed based on the measurement with the machine learning model, taking advantage of the simplified matrix multiplications.

Two machine learning-based approaches using pulse injection to augment SoC estimation have been considered as candidates to update SoC estimation. 1) The machine learning model is continuously operating to obtain the SoC values. However, it usually takes 6-8 minutes[9] for one-time SoC calculation due to the matrix multiplications of the machine learning model is very time-consuming, which hence makes this approach not applicable for real-time SoC estimation. 2) machine learning model only operates at certain moments, for example when the vehicle stops at red light. Between the times when SOC estimation is updated by machine learning, other SoC estimation techniques (such as coulomb-counting and EKF) can be applied to estimate SoC for those cost- and computation-constrained applications.

---

[9] Implement on BeagleBone Black, with Python 3.

Fig. 26 showcases how the latter method is employed in the actual battery system with UDDS driving cycle, which represents a city driving condition for vehicle testing. The red line represents the actual SoC. The blue one illustrates the SoC estimation algorithm of the latter approach, where SoC resets at every point when the electric vehicle stops. After the vehicle restarts, other SoC estimation technique (such as coulomb-counting or EKF) resumes. As a result, accumulated error in the previous driving period will be eliminated. Please note that the error presented between the two SoC curves, in Fig. 26, is exaggerated for greater clarity. In practice, the difference between them will be heavily dependent on the SoC estimation strategy adopted in the system and can be reduced significantly by correcting the estimated SoC more regularly.
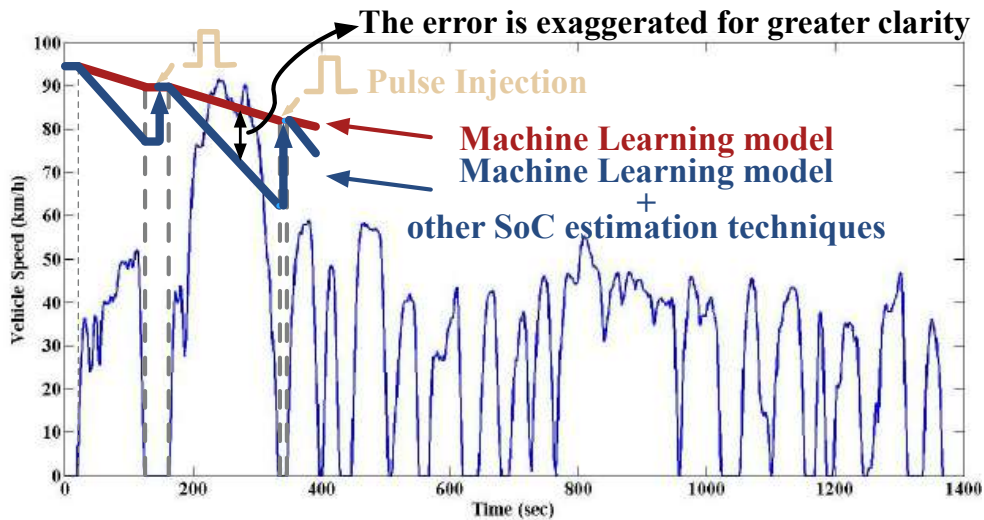
Figure 26: Machine learning approach implemented with UDDS driving cycle.

A summary of the way how three SoC estimation techniques, including coulomb-counting, OCV mapping and machine learning-based method are employed and compared is evident in Fig. 27.
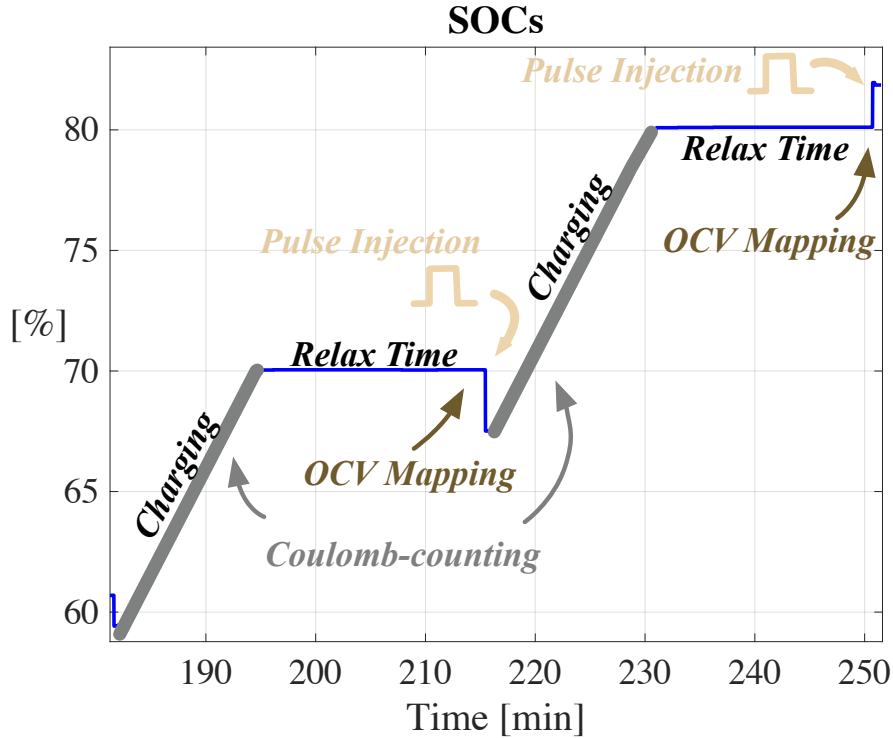
Figure 27: Three SoC Estimation techniques implemented in charging.

Coulomb-counting is used during the whole charging/discharging period as the basis of evaluating the performance of both OCV Mapping and machine learning-based method since the current sensors can achieve less than 0.1% error in the laboratory environment. OCV Mapping is then applied to get the SoC with the voltage measurement that has been relaxed after 90 minutes relax time. Finally, a pulse is injected to retrieve an input of the machine learning model.

3.3.3 Machine Learning Update Module

The applied machine learning model has a structure of two hidden layers, with fully connected nodes on each layer. The input of the model is 1799 battery voltage points that collected during a three minutes pulse at a 10Hz sampling rate and the output is the estimated SoC value for specified input. In order to combine the machine learning model with present testbench, the weights and biases of the FNN are saved in higher-level controller for SoC computation. The diagram of the utilized feedforward neural network (FNN) is shown in Fig. 28,

this FNN can be summarized by a sequence of matrix multiplications and can be represented by following composite functions:
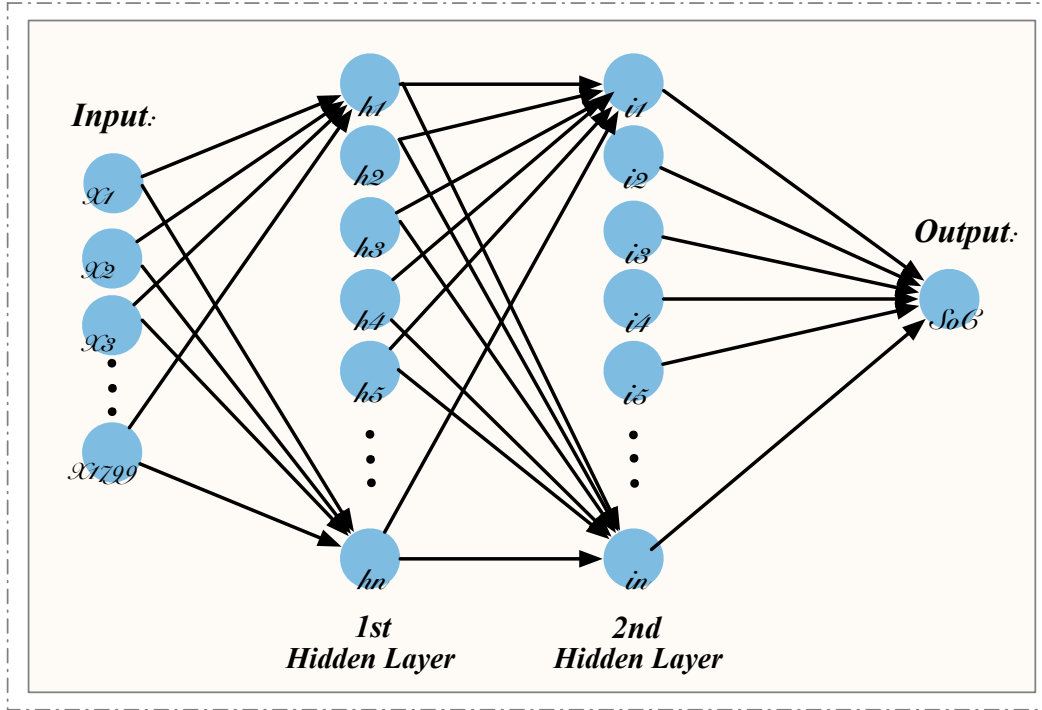
Figure 28: Diagram of the 2-hidden-layer neural network.

$$h_k^l(p) = \eta \left(\sum_k \left(w_{j,k}^l, h_k^{l-1}(p) + b_k^l \right) \right) \tag{24}$$

$$h_k^l(p) = SoC(p), \qquad for \ l = L \tag{25}$$

$$\eta = \max(0, h) \tag{26}$$

$$e(p) = SoC(p) - SoC^*(p) \tag{27}$$

where $w_{j,k}^l$ denote the weight connection between neuron j in layer l -1 and neuron k in layer l. Let b_k^l and h_k^l be the bias and the temporary outcome, respectively, of neuron k in layer l. $SoC(p)$ is the estimated state-of-charge for pulse-train p. The nonlinearity, denoted as η, used in these networks is called Rectified Linear Units (ReLU) due to its simplicity during the

38

feedforward and backpropagation steps. The error signal measuring similarity of the estimated

SoC value to the ground-truth value is $e(p)$.

Figure 29 is the flow diagram of the SoC estimation that depicts the procedure described

in Eq. (24)-(27).
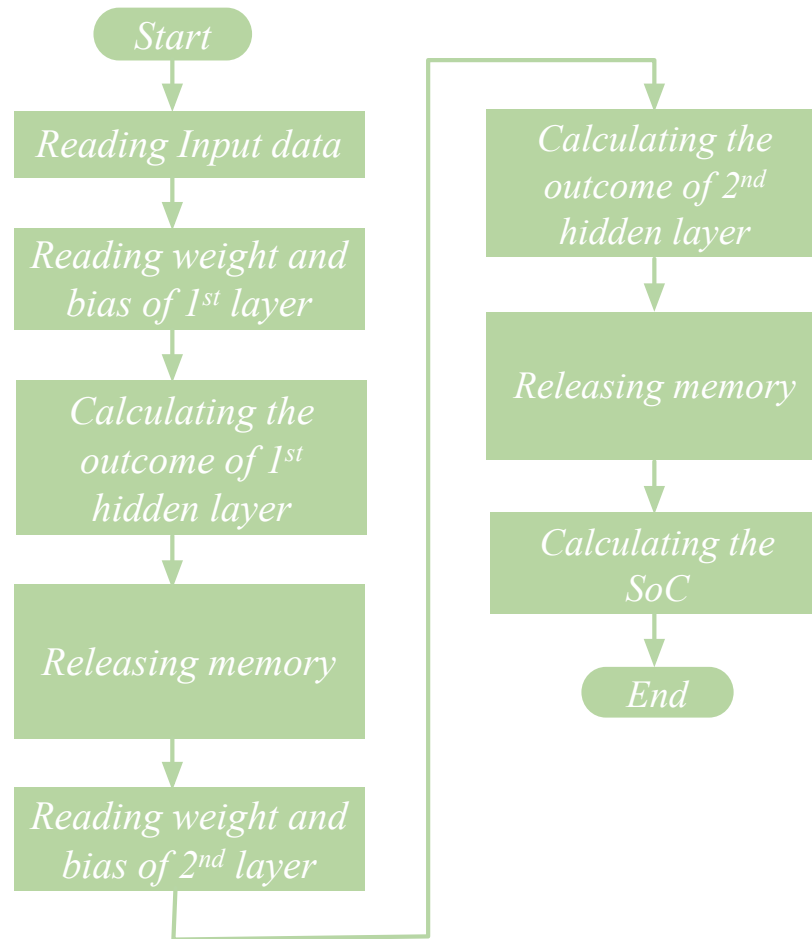
Figure 29: Flowchart of SoC calculation by 2-hidden-layer neural network.

Chapter 4: Experimental Results

In this chapter, the procedure of experiments and results are described and summarized. The entire experiment process is divided into (i) Data extraction for producing the OCV-SoC curves of both charging and discharging environments; (ii) Evaluation for OCV Mapping approach; (iii) Training and validation process for machine learning; and (iv) Comparison between FNN and OCV Mapping.

4.1 OCV-SoC curves

To generate OCV-SoC curves used in further OCV Mapping evaluation experiments under both charging and discharging conditions, the test data collected by the cycler is also categorized into charge- and discharge-data, as presented as the blue lines in Fig. 30 and Fig. 31, respectively. The test data then is fitted by a 6th-order polynomial curve fitting in order to generate fitted data curves, which are plotted as the orange lines in Fig. 30 and Fig. 31.

When OCV Mapping is applied, for every OCV value, a SoC can be calculated with the given 6th-order polynomial as follows:

$$p(x) = p_1x^6 + p_2x^5 + p_3x^4 + p_4x^3 + p_5x^2 + p_6x^1 + p_7 \tag{28}$$

$$p(x) = SoC \tag{29}$$

$$x = OCV \tag{30}$$

The fitted curves hence can be expressed as 6th-order polynomial equations and the coefficient arrays selected for charging and discharging OCV-SoC curves are presented in Table 2.

Table 2: Coefficient arrays of charging and discharging OCV-SoC curves.

	p1	p2	p3	p4	p5	p6	p7
Charge	2.89	-58.50	490.03	-2175.03	5395.70	-7094	3862.32
Discharge	0.35	-7.31	62.31	-281.10	708.24	-945.44	522.60
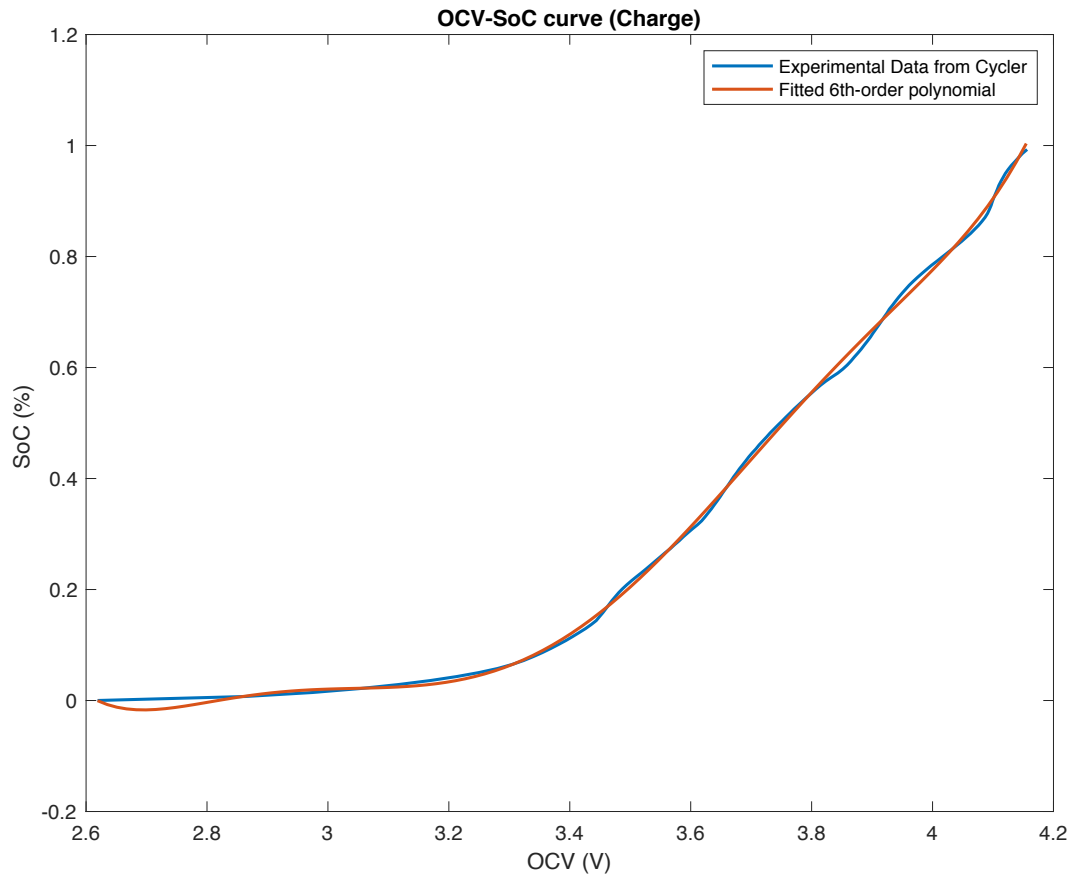
Figure 30: OCV-SoC curve under charging.
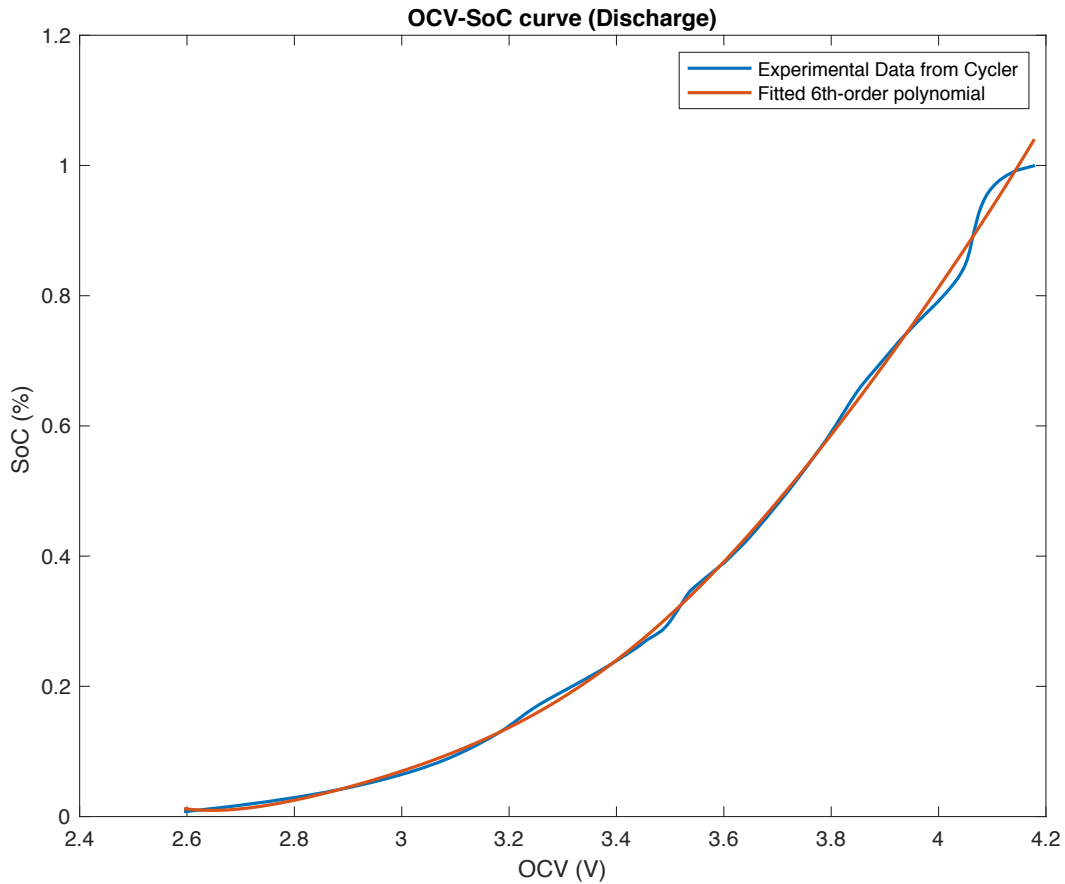
Figure 31: OCV-SoC curve under discharging.

4.2 Performance of OCV Mapping

In order to evaluate the performance of OCV Mapping, comparisons between coulomb-counting and OCV Mapping under both charging and discharging are made. Two batteries cells in the proposed testbench are first charged from 0% SoC to 90% SoC, then discharged to empty, applying 1 C-rate constant current. For every 10% drop/increase in SoC in the testing process, the batteries are relaxed for 90 minutes, letting the sensed voltage to be relaxed to a stable value, which is the OCV. The OCV Mapping result is hence derived from this stable OCV and calculated with the given charge/discharge polynomial. Then the two cells are

charged/discharged for another 10% SoC and repeat the same sequence as aforementioned. This procedure keeps repeating until cut-off voltage is reached at any time.

In Fig. 32 and Fig. 33, for one battery cell, only coulombs are calculated to achieve SoC estimation, as the blue lines in figures; the red lines represent the SoC change of the other cell, where coulomb-counting is used through discharging/charging period, and OCV Mapping is applied after 90 minutes relax time. The error of OCV Mapping, can be seen as the difference between the red and blue line in figures, is defined as the difference between the SoC derived from OCV Mapping and the SoC calculated from coulomb-counting.
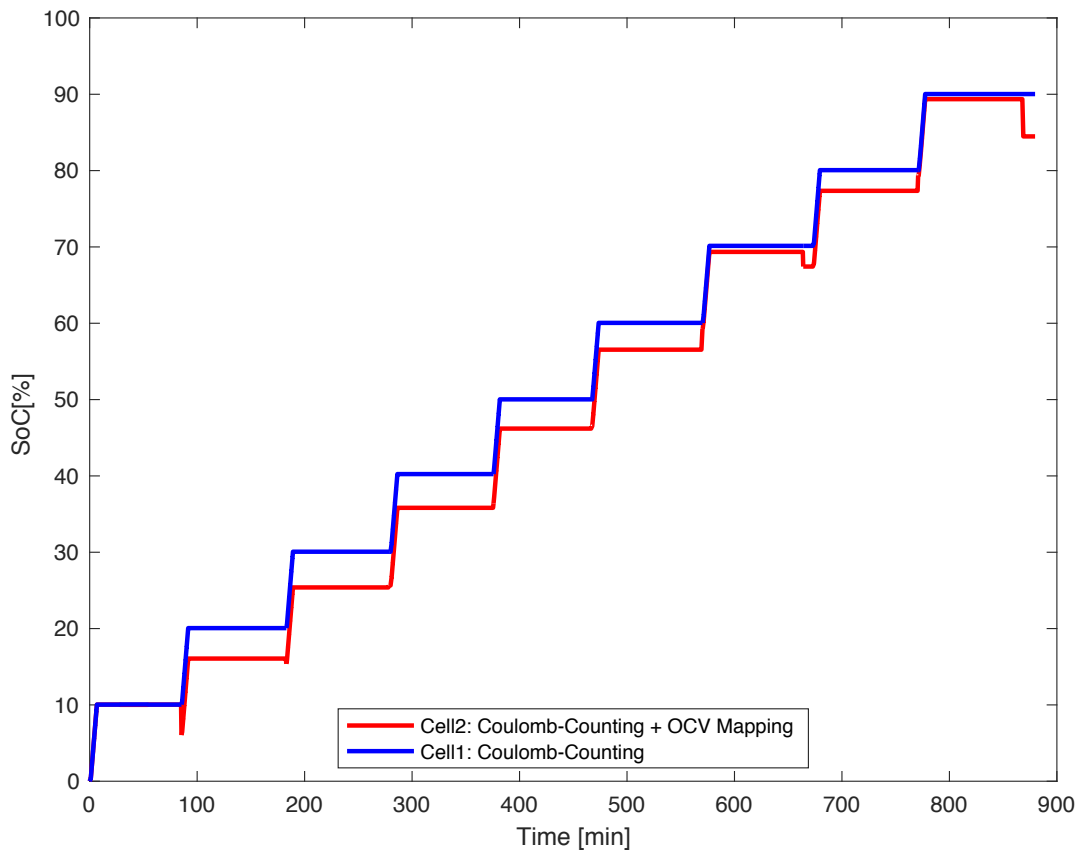
Figure 32: Experimental results of OCV Mapping under charging.
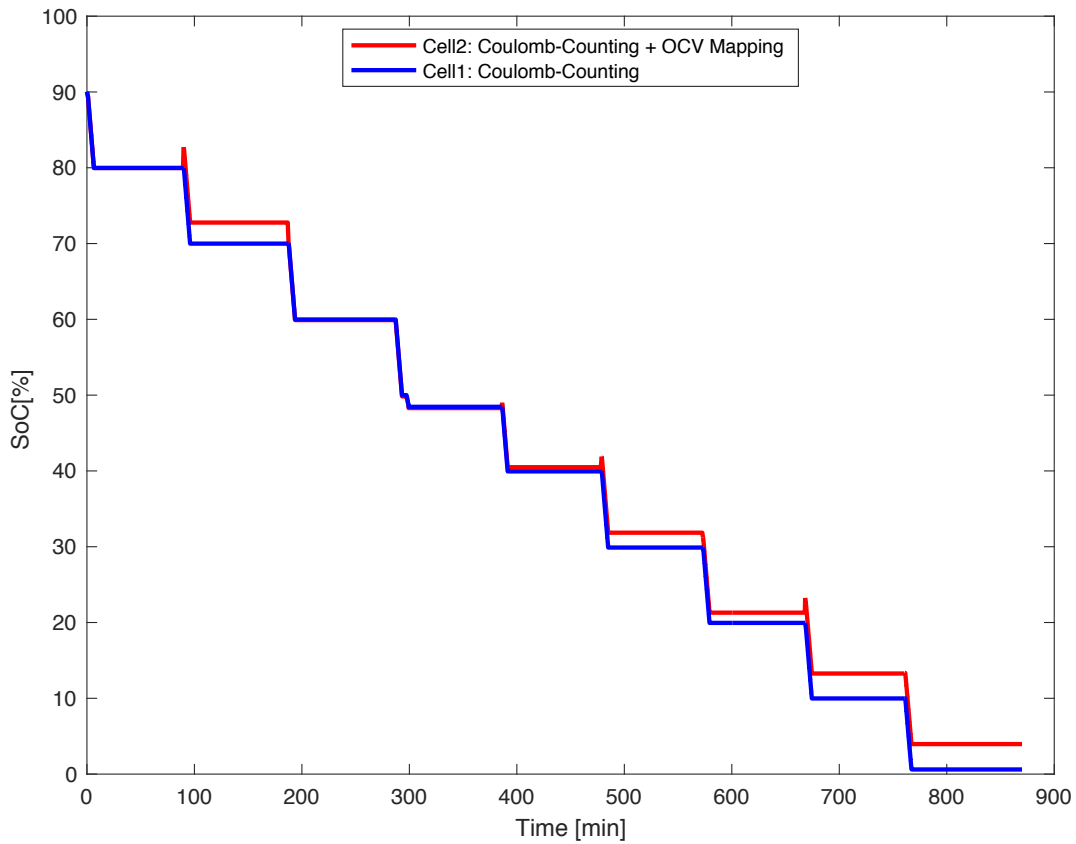
Figure 33: Experimental results of OCV Mapping under discharging.

From Figure 32, the error of OCV Mapping can vary from 0.68% to 5.55%, while the error under discharging changes from 0.2% to 3.43%, as can be seen in Fig. 33. The mean absolute errors (MAEs) of OCV Mapping with 90-minutes relaxations during charging and discharging are 3.35% and 1.86%, respectively.

The currents, voltages and SoCs when charging the batteries from 0% SoC to 90% SoC and discharging the batteries from 90% SoC to 0% SoC under 1 C-rate constant current are plotted in Fig. 34 and Fig. 35, respectively.
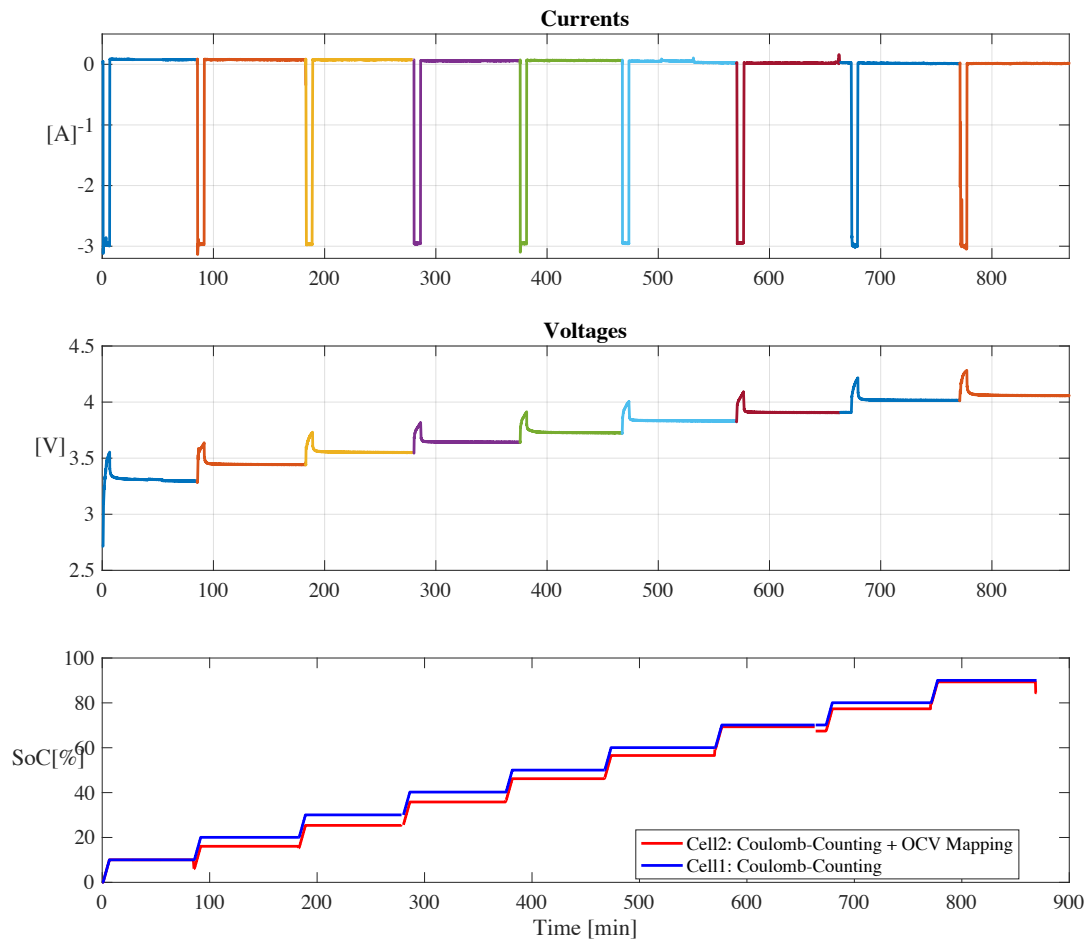
Figure 34: Currents, Voltages and SoCs during charging.
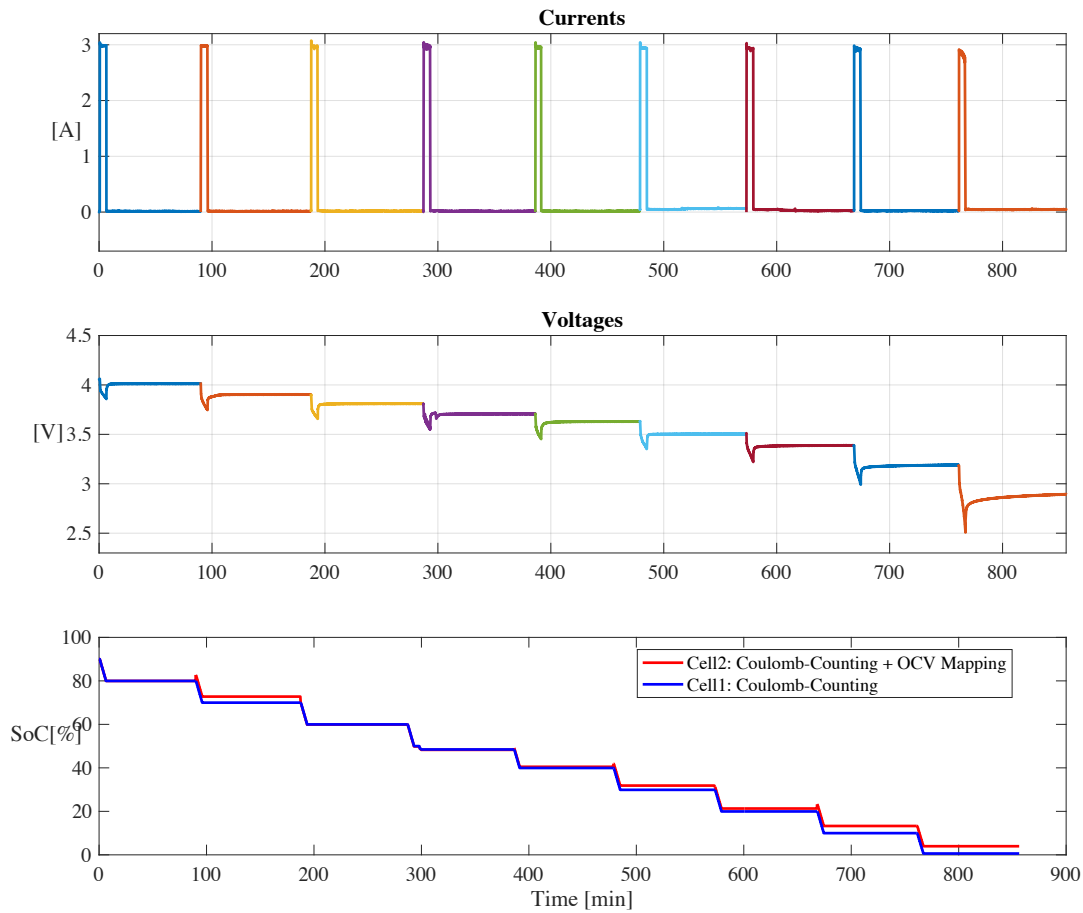
Figure 35: Currents, Voltages and SoCs during discharging.

Typically, the sensed voltage is oscillated after discharging/charging and thus need time to be relaxed to the open-circuit voltage (OCV). The performance of OCV Mapping is investigated from the dependency on length of relax time, which is beneficial to making a trade-off between accuracy and pace, a reasonable time for battery relaxation hence can be selected. As a result, by generating these error figures, we had some confidence and inference about the time we need to wait for battery relaxation and how much accuracy has been achieved with given relax time. The error of OCV Mapping during the relax time under charging and discharging is presented in Fig. 36 and Fig. 37, respectively.
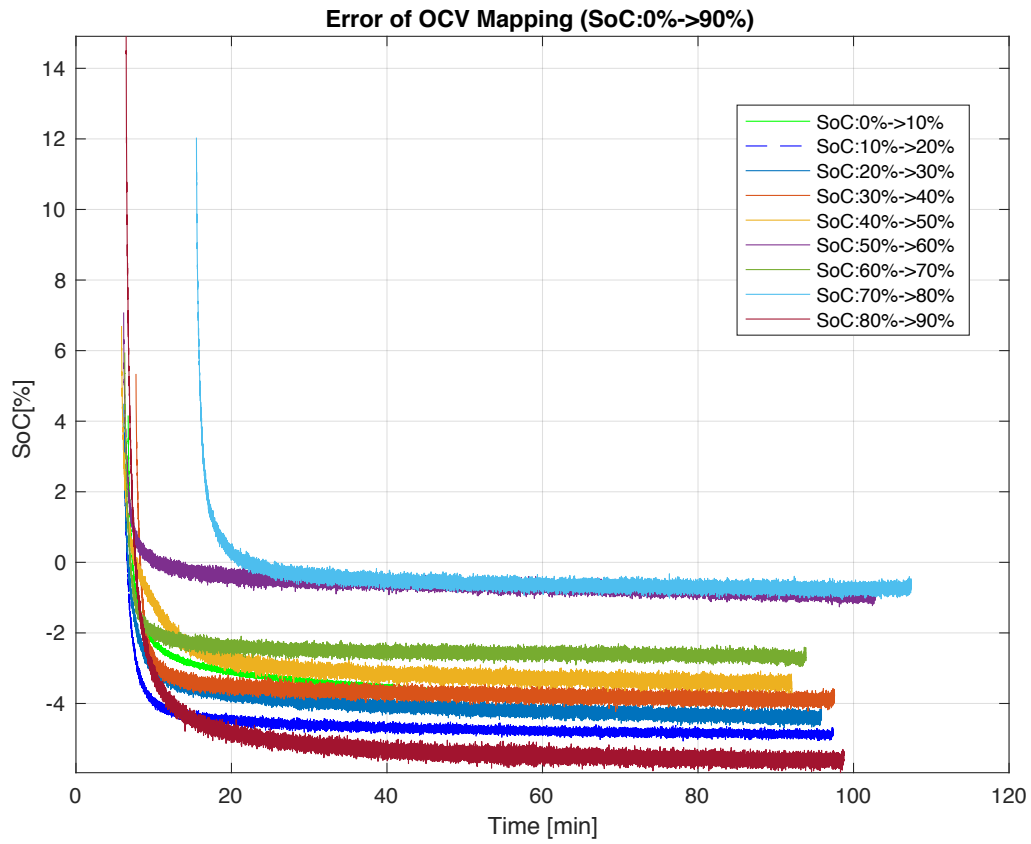
Figure 36: Error of OCV Mapping versus. Relax Time when charging.
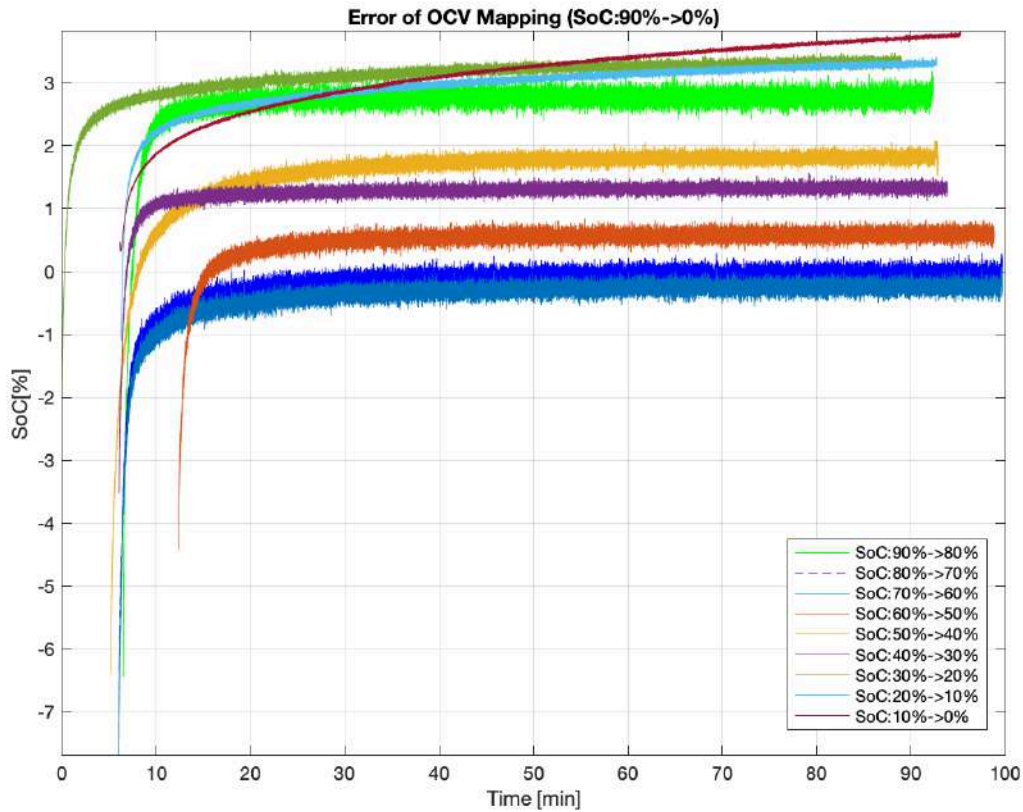
Figure 37: Error of OCV Mapping versus. Relax Time when discharging.

From the results, a minimum of 30 minutes relax time is necessary in order to obtain a relatively reliable result. However, the error after 30 minutes relaxation still has a difference with the end point error, this difference is usually within 1%.

4.3 Training for Machine Learning Model

Training of the FNN is operated with test data that captured by the cycler and is done offline and only when network converges to a lower loss threshold can the networks be applied online. During online operation, only a forward pass is required in order to estimate SoC. Backward passes are no longer required once the model is appropriately trained. FNNs offer an advantage of faster computing time, once trained, since a forward pass is comprised mainly of a sequence of matrix multiplications.

In this section, TensorFlow (Abadi et al., 2015), a machine learning framework, is used with a TITAN Xp NVIDIA Graphical Processing Unit (GPU). The TensorFlow and Keras frameworks provide the ability to prototype neural networks quickly and iterate on various architectures and loss functions. These frameworks also offer automatic gradient computation thereby allowing for a seamless backward computation without any manual intervention.

4.4 Input of Machine Learning Model

As aforementioned, the proposed hypothesis of the project is that passing current pulses through a battery and measuring the voltage response to these pulses can be used to improve the robustness of SoC estimation.

The test procedure is similar to the steps of implementing OCV Mapping. The pulses are injected at every 10% drop/increase in SoC in the testing process. Two batteries cells in the proposed testbench are first charged from 0% SoC to 90% SoC, then discharged to empty, applying 1 C-rate constant current. For every 10% drop/increase in SoC, the batteries are relaxed for 1-hour, allowing complete equilibrium inside of the battery. By allowing 1-hour relaxation before injecting pulses, the voltage response isolates the charge-transfer and/or charge diffusion effects that are induced by previous current excitation. The subsequent voltage response will be purely excited by the current pulses. If the cell is not well rested, the charge history will be coupled into the pulse response, which makes the results less accurate. The voltage response is captured as the input of the machine learning model, including 1799 voltage points that sampled at 10Hz during this 3-mins pulse. After pulse injection, the two cells are charged/discharged for another 10% SoC and repeat the same procedure. The sample inputs for machine learning model is shown in Fig. 38.
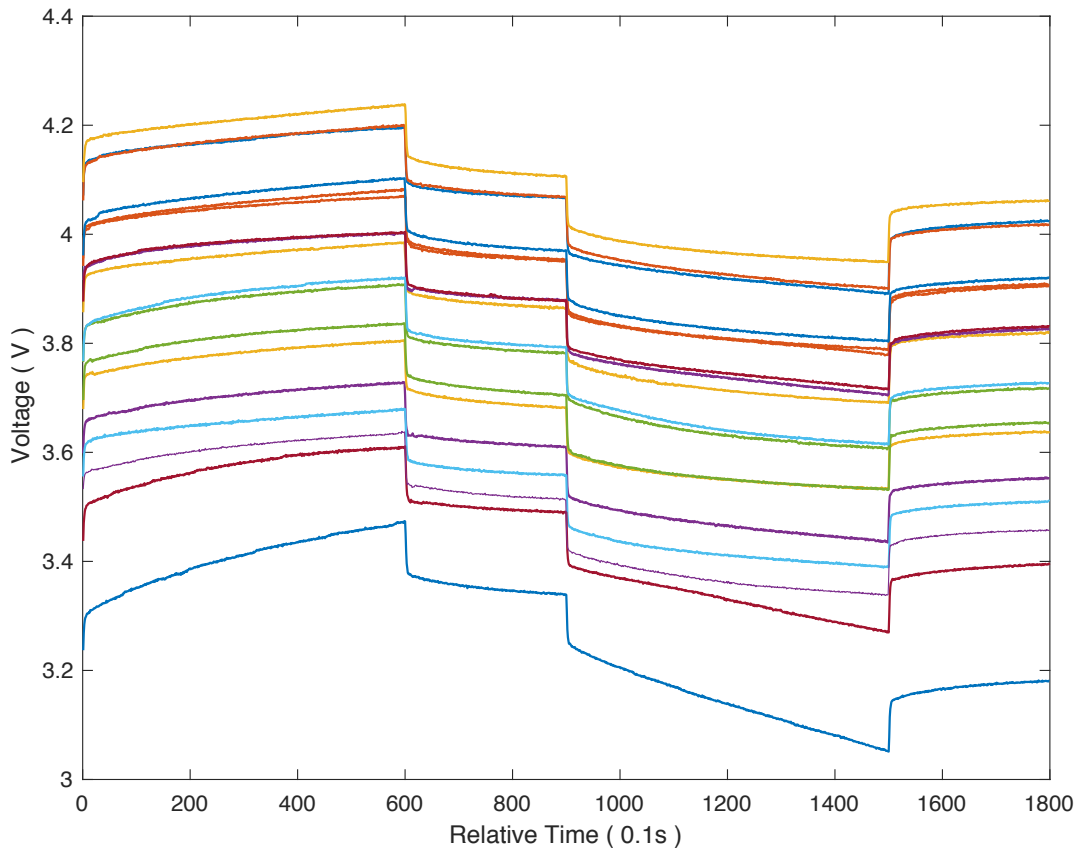
Figure 38: Sample Inputs for machine learning model, including voltage responses from both charge and discharge.

4.5 SoC Calculation in BeagleBone Black

The validation process combining the FNN with present testbench is comprised mainly of a sequence of matrix multiplications. Based on the 2-hidden layer structure of the machine learning model, three weight- and three bias- arrays that attributes to this model are extracted as six csv files and saved into BeagleBone Black for SoC calculation. The program that implements the multiplication of matrices is wrote in Python, numpy package provides the capability of processing large amounts of data in a rapid manner.

The computing time varies according to the number of nodes in each layer. For instance, a model that contains 4000 nodes on each hidden layer often takes 10 minutes for one-time SoC

calculation; whereas 8 minutes is needed for a model with 2400 nodes in each layer, a 300-node-model only demands 90 second. However, the more nodes in each layer contributes to a more accurate SoC result. The mean-absolute errors of the aforementioned models from all test data are 1.12%, 1.13% and 3.27%, independently. For these reasons, a trade-off has been made between computation time and accuracy. In this thesis, the number of nodes in each hidden layer for charge is chosen to be 2400 since it can achieve the precise estimation result while keeping reasonable computation time. The size of FNN for discharge is selected to be 2500 nodes on each hidden layer, it is capable of achieving 0.80% MAE.

4.6 Comparison between OCV Mapping and Machine Learning-based method

As discussed previously, the MAEs of two FNNs for charge and discharge are 1.13% and 0.80%, separately, while the MAEs of OCV Mapping with 90-minutes relaxations during charging and discharging are 3.35% and 1.86%, respectively. The 3-mins pulse is injected after 90 minutes battery relaxation, the OCV Mapping is applied before the pulse injection as to compare the SoC results obtained from two methods. The comparison processes and results of charge and discharge are indicated in Fig. 39 and Fig. 40, respectively. The charge- and discharge- error at every SoC level of machine learning model and OCV Mapping are presented in Fig. 41 and Fig. 42, separately. The error shown in figures at each SoC level is the average error at this SoC value from all test data.

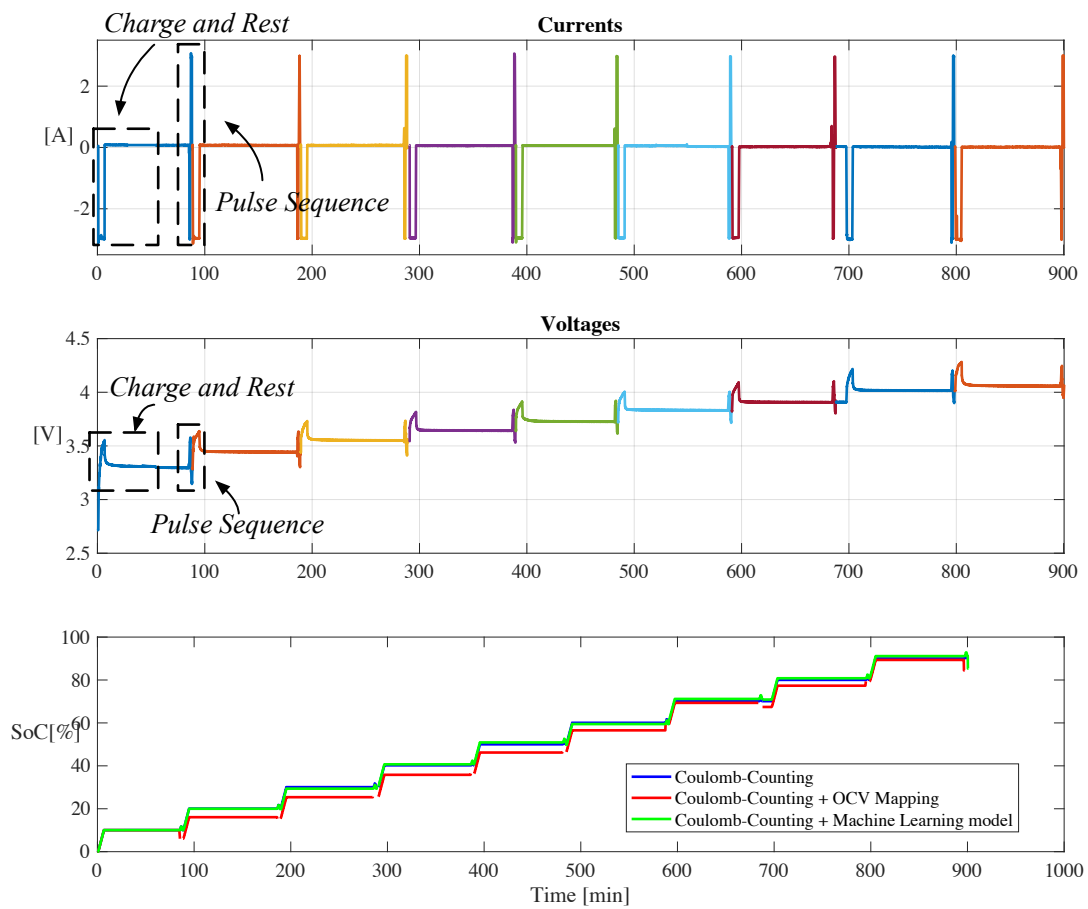**Figure 39: Comparison between OCV Mapping and machine learning-based approach during charging.**
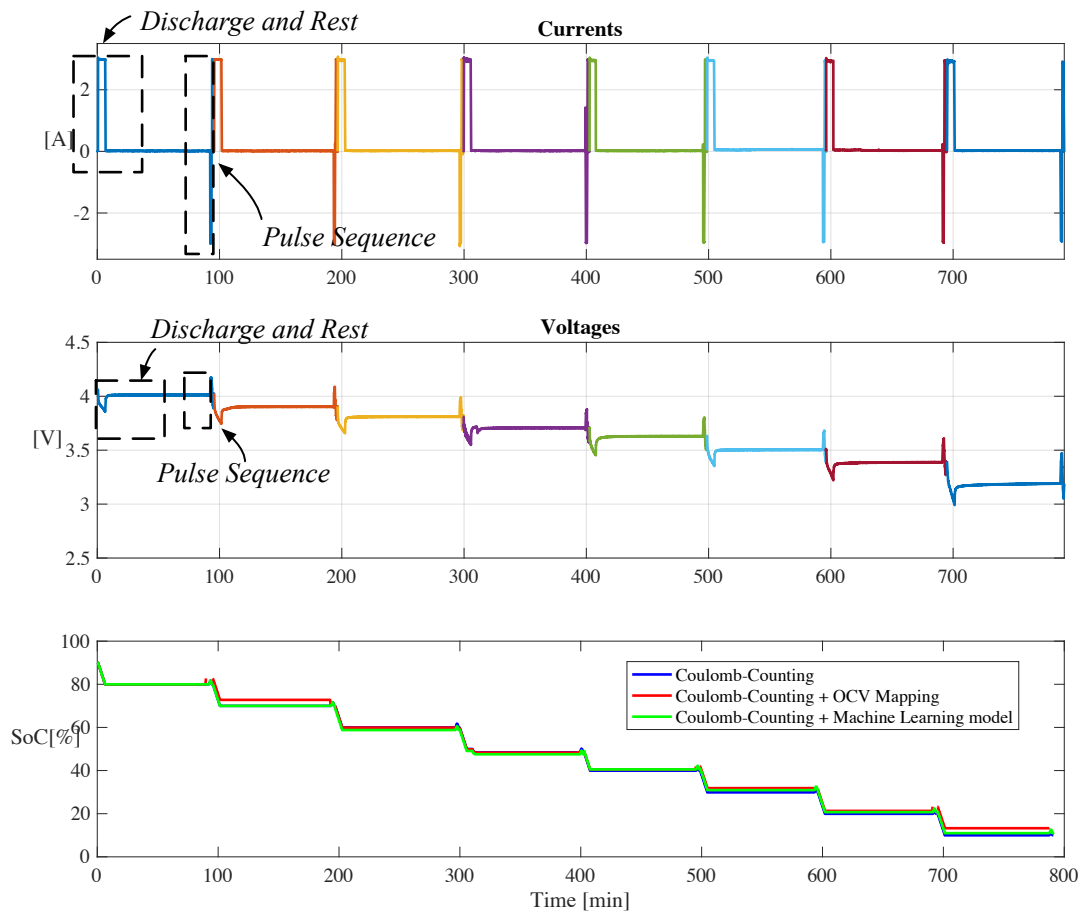
Figure 40: Comparison between OCV Mapping and machine learning-based approach during discharging.
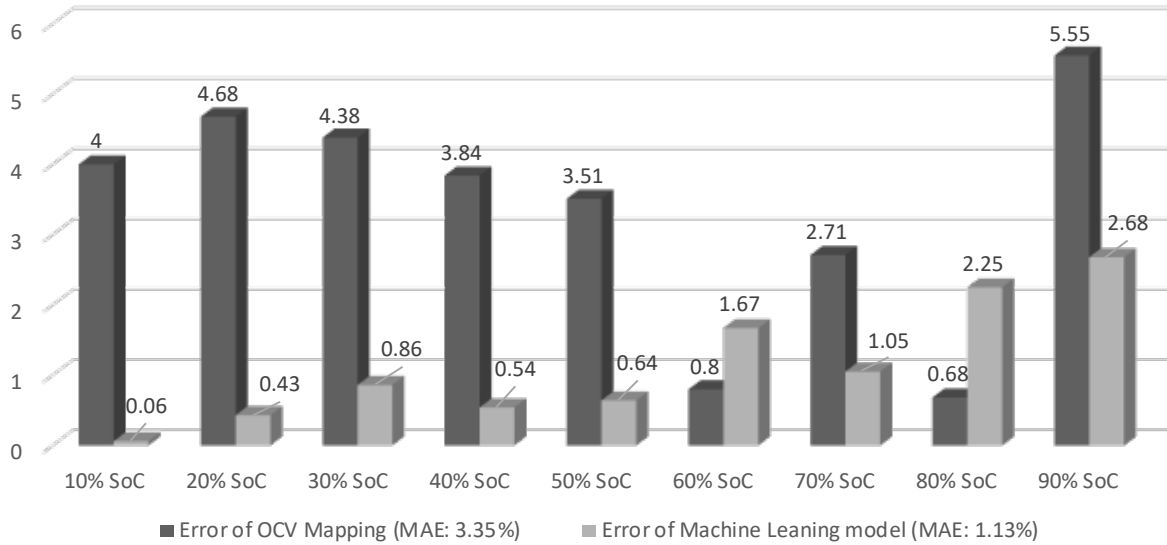
Figure 41: Average Error of OCV Mapping and machine learning-based approach at each SoC level during charge.
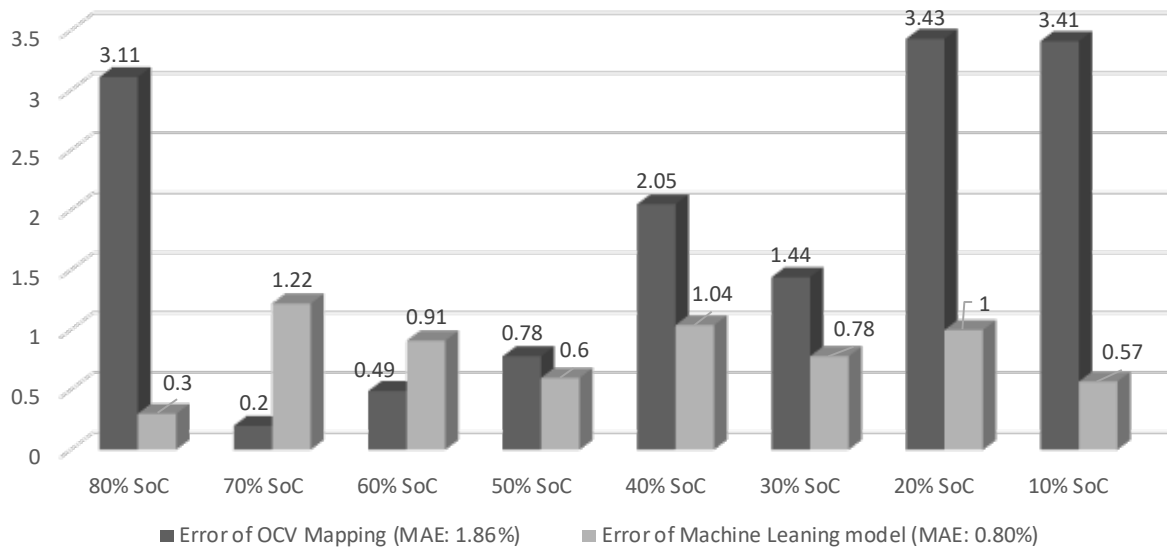
Figure 42: Average Error of OCV Mapping and machine learning-based approach at each SoC level during discharge.

Conclusion

This thesis introduces a new strategy to augment the performance of SoC estimation powered by neural networks. A 2-hidden layer structure is used and the concept of the pulse injection is demonstrated to achieve the high-fidelity SoC estimation. OCV Mapping is also employed in order to evaluate and compare the performances with machine learning-based approach. Coulomb-counting is selected as the basis of comparison as it is capable of obtaining SoC with an error less than 0.1%. The real-world testbench composing of a battery balancing circuit, a TI controller and a Beaglebone Black is introduced, where a pulse injection can be integrated into balancing current demands without interfering with driving behaviors. Testing procedures tailored for both OCV Mapping and machine learning-based approach are discussed and detailed steps are given. The method to construct FNN for mapping the pulse measurements to a ground-truth is provided. By applying FNN to the data, the SoC can be reconstructed within an error boundary of 1.13% during charge and 0.80% during discharge, whereas OCV Mapping has an error of approximately 3.35% for charging and 1.86% for discharging. Thanks to the advantage of FNN, a BeagleBone Black is capable of calculating SoC with just simplified matrix multiplications in 6-8mins given a well-tuned model, which tremendously cut the time cost to one tenth of OCV Mapping.

References

Eberle, U. and Helmolt, V.R. *Sustainable transportation based on electric vehicle concepts: a brief overview*. Energy and Environmental Science, 2010.

Situ, L.X. *Electric Vehicle Development: The Past, Present and Future*. In 2009 International Conference on Power Electronics Systems and Applications, 2009.

Chan, C.C. *The State of the Art of Electric and Hybrid Vehicles*. Proceedings of the IEEE, Vol. 90, NO. 2, Feb. 2002.

Woodward, M. *Deloitte: Battery Electric Vehicles*. Available online: https://www2.deloitte.com/content/dam/Deloitte/uk/Documents/manufacturing/deloitte -uk-battery-electric-vehicles.pdf. 2008

Carley, D. The Beginners Guide to Electric Vehicles (EV), 2014.

Dunn, B., Kamath, H. and Tarascon, J.M. *Electrical Energy Storage for the Grid: A Battery of Choices.* Science 334, 928, Nov. 2011.

Li, C.R., Xiao, F. and Fan, Y.X. *An Approach to State of Charge Estimation of Lithium-Ion Batteries Based on Recurrent Neural Networks with Gated Recurrent Unit.* Energies, 1592, Dec. 2019.

Zaghib, K., Mauger, A. and Julien, C.M. *Rechargeable Lithium Batteries: From Fundamentals to Applications.* In Woodhead Publishing, pp.319-351, 2015.

Cheng, K.W.E., Divakar, B.P., Wu, H., Ding, K. and Ho, H.F. *Battery-Management System (BMS) and SOC Development for Electrical Vehicles. In IEEE Transactions on Vehicular Technology*, Vol. 60, No. 1, pp.76-88, Jan. 2011.

Rahimi, E.H., Ojha, U., Baronti, F. and Chow, M. *Battery Management System: An Overview of Its Application in the Smart Grid and Electric Vehicles*. In IEEE Industrial Electronics Magazine, Vol. 7, No. 2, pp.4-16, Jun. 2013.

Brandl, M. et al. *Batteries and battery management systems for electric vehicles*. Dresden: 2012 Design, Automation & Test in Europe Conference & Exhibition (DATE), pp.971-976, 2012.

Shun, X., Guangdi, HuRuisen, H., Feng, G. and Pengkai, Z. *Lithium-Ion Battery Online Rapid State-of-Power Estimation under Multiple Constraints*. Energies, 283, Nov. 2018.

Remmlinger, J., Buchholz, M., Meiler, M., Bernreuter, P. and Dietmayer, K. *State-of-health monitoring of lithium-ion batteries in electric vehicles by on-board internal resistance estimation. Journal of Power Sources*, Vol. 196, No. 12, pp.5357–5363, 2011.

Lee, S., Kim, J., Lee, J. and Cho, B.H. *State-of-charge and capacity estimation of lithium-ion battery using a new open-circuit voltage versus state-of-charge*. Journal of Power Sources, Vol. 185, No. 2, pp.1367–1373, 2008.

Pang, S., Farrell, J., Du, J. and Barth, M. *Battery state-of-charge estimation*. In American Control Conference, Proceedings of the 2001, IEEE, Vol. 2, pp.1644–1649, 2001.

Piller, S., Perrin, M. and Jossen, A. *Methods for state-of-charge determination and their applications.* Journal of Power Sources, Proceedings of the 22nd International Power Sources Symposium, Vol. 96, No. 1, pp.113–120, 2001.

Chemali, E., Preindl, M., Malysz, P. and Emadi, A. *Electrochemical and electrostatic energy storage and management systems for electric drive vehicles: State of the art review and future trends.* IEEE Journal of Emerging and Selected Topics in Power Electronics, Vol. 4, pp.1117–1134, 2016.

Waag, W., Fleischer, C. and Sauer, D.U. *Critical review of the methods for monitoring of lithium-ion batteries in electric and hybrid vehicles*. Journal of Power Sources, Vol. 258, pp.321–339, 2014.

Baronti, F., Fantechi, G., Fanucci, L., Leonardi, E., Roncella, R., Saletti, R. and Saponara, S. *State-of-charge estimation enhancing of lithium batteries through a temperature-dependent cell model*. International Conference on Applied Electronics, Vol. 0, No. 1, pp.29–34, 2011.

Roscher, M.A., Bohlen, O. and Vetter, J. *OCV Hysteresis in Li-Ion Batteries including Two-Phase Transition Materials*. International Journal of Electrochemistry, Vol. 2011, pp.1–6, 2011. arXiv: ID984320.

Waag, W., Fleischer, C. and Sauer, D.U. *Adaptive on-line prediction of the available power of lithium-ion batteries*. Journal of Power Sources, Vol. 242, pp.548–559, 2013.

Xiong, R., Cao, J., Yu, Q. and Sun, F. *SPECIAL SECTION ON BATTERY ENERGY STORAGE AND MANAGEMENT SYSTEMS Critical Review on the Battery State of Charge Estimation Methods for Electric Vehicles*. IEEE Access, Vol. 6, pp.1832–1843, 2017.

Ng, K.S., Moo, C.S., Chen, Y.P. and Hsieh, Y. C. *Enhanced coulomb counting method for estimating state-of-charge and state-of-health of lithium-ion batteries*. Applied Energy, Vol. 86, No. 9, pp.1506–1511, 2009.

Baccouche,I., Jemmali, S., Mlayah, A., Manai, B. and Amara, E.B.N. *Implementation of an Improved Coulomb-Counting Algorithm Based on a Piecewise SOC-OCV Relationship for SOC Estimation of Li-Ion Battery*. INTERNATIONAL JOURNAL of RENEWABLE ENERGY RESEARCH, Vol.8, No.1, Mar. 2018.

Lai, X., Zheng, Y. and Sun, T. *A comparative study of different equivalent circuit models for estimating state-of-charge of lithium-ion batteries*. Electrochim, 259, pp.566–577, 2018.

Han, J., Kim, D. and Sunwoo, M. *State-of-charge estimation of lead-acid batteries using an adaptive extended Kalman filter*. Journal of Power Sources, Vol. 188, No. 2, pp.606–612, 2009.

He, H., Xiong, R., Zhang, X., Sun, F. and Fan, J. *State-of-charge estimation of the lithium-ion battery using an adaptive extended Kalman filter based on an improved Thevenin model*. IEEE Transactions on Vehicular Technology, Vol. 60, No. 4, pp.1461–1469, May. 2011.

Kim, J. and Cho, B.H. *State-of-charge estimation and state-of-health prediction of a Li-ion degraded battery based on an EKF combined with a per-unit system*. IEEE Transactions on Vehicular Technology, November, Vol. 60, No. 9, pp.4249–4260, 2011.

Plett, G.L. *Extended Kalman filtering for battery management systems of LiPB-based HEV battery packs: part 1. Background*. Journal of Power Sources, Vol. 134, No. 2, pp.252–261, 2004.

Plett, G.L. *Extended Kalman filtering for battery management systems of LiPB-based HEV battery packs: part 2. Modeling and identification*. Journal of Power Sources, Vol. 134, No. 2, pp.262–276, 2004.

Plett, G.L. *Extended Kalman filtering for battery management systems of LiPB-based HEV battery packs: part 3. State and parameter estimation*. Journal of Power Sources, Vol. 134, No. 2, pp.277–292, 2004.

Rubagotti, M., Onori, S. and Rizzoni, G. *Automotive battery prognostics using dual extended Kalman filter*. In ASME 2009 Dynamic Systems and Control Conference, pp.257–263, 2009.

Taborelli, C. and Onori, S. *State of charge estimation using extended Kalman filters for battery management system*. In 2014 IEEE International Electric Vehicle Conference, Dec. 2014.

Vasebi, A., Partovibakhsh, M. and Taghi Bathaee, S.M. *A novel combined battery model for state-of-charge estimation in lead-acid batteries based on extended Kalman filter for hybrid electric vehicle applications*. Journal of Power Sources, Vol. 174, No. 1, pp.30–40, 2007.

Arasaratnam, I. and Haykin, S. *Cubature kalman filters*. Autom. Control. IEEE Transactions, No. 7, pp.1–16, 2009.

Afshari, H.H., Gadsden, A., Ahmed, R. and Habibi, S. State of Charge *Estimation of Li-Ion Batteries Using the Dynamic 2nd Order Smooth Variable Structure Filter*. 25th Canadian Congress of Applied Mechanics (CANCAM 2015), 2015

Habibi, S. *The smooth variable structure filter*. Proc. IEEE, Vol. 95, No. 5, pp.1026–1059, 2007.

Domenico,D.D., Fiengo, G. and Stefanopoulou, A. *Lithium-ion battery state of charge estimation with a Kalman Filter based on an electrochemical model*. Control Appl. 2008. CCA 2008. IEEE Int. Conf., pp.702–707, 2008.

Ahmed, R., Sayed, E.M., Arasaratnam, I., Tjong, J. and Habibi, S. *Reduced-Order Electrochemical Model Parameters Identification and SOC Estimation for Healthy and Aged Li-Ion Batteries. Part I: Parameterization Model Development for Healthy Batteries*. IEEE J. Emerg. Sel. Top. Power Electron., Vol. 2, No. 3, pp.659–677, 2014.

Speltino, C., Domenico,D.D., Fiengo, G. and Stefanopoulou, A. *Comparison of reduced order lithium-ion battery models for control applications*. Proc. 48h IEEE Conf. Decis. Control held jointly with 2009 28th Chinese Control Conf., pp.3276–3281, 2009.

Welch, G. and Bishop, G. *An Introduction to the Kalman Filter*. Chapel Hill, NC, USA: University of North Carolina at Chapel Hill, 1995.

Hua, X. Li, S., Peng, H. and Sun, F. *Robustness analysis of state-of-charge estimation methods for two types of Li-ion batteries*. J. Power Sources, 217, pp.209–219, 2012.

He, Z.W., Gao, M.Y., Wang, C.S., Wang, L.Y. and Liu, Y.Y. *Adaptive state of charge estimation for Li-ion batteries based on an unscented Kalman filter with an enhanced battery model*. Energies, pp.4134–4151, Jun. 2013.

Li, J., Barillas, J.K., Guenther, C. and Danzer, M.A. *A comparative study of state of charge estimation algorithms for LiFePO4 batteries used in electric vehicles*. J. Power Sources, 230, pp.244–250, 2013.

Du, J., Liu, Z. and Wang, Y. State of charge estimation for Li-ion battery based on model from extreme learning machine. Control Engineering Practice, Vol. 26, No. 1, pp.11–19, 2014.

Zhang, S.S., Xu, K. and Jow, T.R. *Electrochemical impedance study on the low temperature of Li-ion batteries.* Electrochimica Acta, Vol. 49, No. 7, pp.1057–1061, 2004.

He, H., Xiong, R., Guo, H. and Li, S. *Comparison study on the battery models used for the energy management of batteries in electric vehicles*. Energy Convers. Manag, 64, pp.113–121, 2012.

Rubio, J. and Pascual, I.A. *Energy-aware broadcast multiuse-MIMO precoder design with imperfect channel and battery knowledge*. IEEE Trans, Wirel, Commun, 13, pp.3137–3152, 2014.

Zheng, L., Jiang, J., Wang, Z. and Zhao, T. *Embedded implementation of SOC estimation based on the Luenberger observer technique*. In Proceedings of the IEEE Conference and Expo Transportation Electrification Asia-Pacific, 2014.

Ning, B., Xu, J., Cao, B. and Xu, G. *A sliding mode observer SOC estimation method based on parameter adaptive battery model*. Energy Procedia, 88, pp.619–626, 2016.

He, H., Zhang, X., Xiong, R., Xu, Y. and Guo, H. *Online model-based estimation of state-of-charge and open-circuit voltage of lithium-ion batteries in electric vehicles*. Energy, Vol. 39, No. 1, pp.310–318, 2012.

Krizhevsky, A., Sutskever, I. and Hinton, G.E. *ImageNet Classification with Deep Convolutional Neural Networks.* Advances in Neural Information Processing Systems, pp.1–9, 2012.

CireAn, D., Meier, U., Masci, J. and Schmidhuber, J. *Multi-column deep neural network for traffic sign classification*. Neural Networks, Vol. 32, pp.333–338, 2012.

Hinton, G., Deng, L., Yu, D., Dahl, G. E., Mohamed, R.A., Jaitly, N., Senior, A., Vanhoucke, V., Nguyen, P., Sainath, T. N. and Kingsbury, B. *Deep neural networks for acoustic modeling in speech recognition: The shared views of four research groups*. IEEE Signal Processing Magazine, Vol. 29, No. 6, pp.82–97, Nov. 2012.

Ma, J., Sheridan, R. P., Liaw, A., Dahl, G. E. and Svetnik, V. *Deep neural nets as a method for quantitative structureactivity relationships*. Journal of Chemical Information and Modeling, Vol. 55, No. 2, pp.263–274, 2015.

Wang, Z.-K., Shu, J., Zhu, Q.-C., Cao, B.-Y., Chen, H., Wu, X.-Y., Bartlett, B. M., Wang, K.-X. and Chen J.-S. *Graphene-nanosheet-wrapped LiV3O8 nanocomposites as high-performance cathode materials for rechargeable lithium ion batteries*. Journal of Power Sources, Vol. 307, pp.426–434, Mar. 2016.

Li, S.G., Sharkh, S.M., Walsh, F.C. and Zhang, C.N. *Energy and battery management of a plug-in series hybrid electric vehicle using fuzzy logic*. IEEE Trans. Veh. Technol, 60, pp.3571–3585, 2011.

Alvarez, A.J.C., Garcia, N.P.J., Blanco, V.C. and Vilan, J.A. *Support vector machines used to estimate the battery state of charge.* IEEE Trans. Power Electr, 28, pp.5919–5926, 2013.

Hu, J.N., Hu, J.J., Lin, H.B., Li, X.P., Jiang, C.L., Qiu, X.H. and Li, W.S. *State-of-charge estimation for battery management system using optimized support vector machine for regression.* J. Power Sources, 269, pp.682–693, 2014.

Eddahech, A., Briat, O. and Vinassa, J.M. *Adaptive voltage estimation for EV Li-ion cell based on artificial neural networks state-of-charge meter*. In Proceedings of the IEEE International Symposium on Industrial Electronics, May. 2012.

Guo, Y., Zhao, Z. and Huang, L. *SoC estimation of Lithium battery based on improved BP neural network.* Energy Procedia, 105, pp.4153–4158, 2017.

Dong, C. and Wang, G. *Estimation of power battery SOC based on improved BP neural network*. In Proceedings of the IEEE International Conference on Mechatronics and Automation, Aug. 2014.

Tong, S., Lacap, J.H. and Park, J.W. *Battery state of charge estimation using a load-classifying neural network.* J. Energy Storage, 7, pp.236–243, 2016.

Hannan, M.A., Lipu, M.S.H., Hussain, A. and Saad, M.H.M. *Neural network approach for estimating state of charge of Lithium-ion battery using backtracking search algorithm.* IEEE Access, pp.10069–10079, Jun. 2018.

Charkhgard, M. and Farrokhi, M. *State-of-charge estimation for lithium-ion batteries using neural networks and EKF*. IEEE Transactions on Industrial Electronics, Vol. 57, No. 12, pp.4178–4187, 2010.

Chemali, E., Kollmeyer, P., Preindl, M. and Emadi, A. *State-of-charge estimation of li-ion batteries using deep neural networks: A machine learning approach.* Journal of Power Sources, Vol. 400, pp.242–255, 2018.

Cuadras, A. and Kanoun, O. *SoC Li-ion battery monitoring with impedance spectroscopy*. 2009 6th International Multi-Conference on Systems, Signals and Devices, pp.1-5, 2009.

Elabadine, Z.D., Ali, M. and Mourad, H. *A Novel Hybrid Technique to Predict the Lithium-Ion Battery's Behavior and Estimate the Intern Impedance.* International Journal of Emerging Electric Power Systems, Jul. 2017.

Zenati, A., Desprez, P. and Razik, H. *Estimation of the SOC and the SOH of li-ion batteries, by combining impedance measurements with the fuzzy logic inference*. IECON 2010 - 36th Annual Conference on IEEE Industrial Electronics Society, pp.1773-1778, 2010.

Zenati, A., Desprez, P., Razik, H. and Rael, S. *Impedance measurements combined with the fuzzy logic methodology to assess the SOC and SOH of lithium-ion cells*. 2010 IEEE Vehicle Power and Propulsion Conference, pp.1-6, 2010.

Waag, W., Käbitz, S. and Sauer, D.U. *Experimental investigation of the lithium-ion battery impedance characteristic at various conditions and aging states and its influence on the application.* Appl. Energy, 102, pp.885-897, 2013.

Ovejas, J.V. and Cuadras, A. *Impedance Characterization of an LCO-NMC/Graphite Cell: Ohmic Conduction, SEI Transport and Charge-Transfer Phenomenon.* Batteries 2018, 4(3), 43, 2018.

Abadi, M., Agarwal, A., Barham, P., Brevdo, E., Chen, Z., Citro, C., Corrado, G. S., Davis, A., Dean, J., Devin, M. et al. *Tensorflow: Large-scale machine learning on heterogeneous systems.* 2015. url: http," Software available from tensorflow.org.

Wang, W., Wang, D., Wang, X., Li, T., Ahmed, R., Habibi, S. and Emadi, A. *Comparison of Kalman Filter-based State of Charge Estimation Strategies for Li-Ion Batteries.* 2006.

Wang, W., Brady, W.N., Liao, C., Fahmy, A.Y., Chemali, E., West, C.A. and Preindl, M. *High-Fidelity State-of-Charge Estimation of Li-Ion Batteries using Machine Learning.* 2019.

Wang, W. *Modeling, Estimation and Benchmarking of Lithium Ion Electric Bicycle Battery.* Master's thesis, Department of Electrical and Computer Engineering, Canada: McMaster University, p.149, 2016.

Wang, W. and Preindl, M. *Dual Cell Links for Battery-Balancing Auxiliary Power Modules: A Cost-Effective Increase of Accessible Pack Capacity.* In IEEE Transactions on Industry Applications, 2019.

Leens, F. *An introduction to I2C and SPI protocols.* In IEEE Instrumentation & Measurement Magazine, Vol. 12, No. 1, pp.8-13, Feb. 2009.

Saha, S., Rahman M. A. and Thakur, A. *Design and implementation of SPI bus protocol with Built-in-self-test capability over FPGA.* 2014 International Conference on Electrical Engineering and Information & Communication Technology, pp.1-6, 2014.

Appendix A

A machine learning model trained with both charge- and discharge- pulses provides relatively accurate outcomes either during charge or discharge, which error at each SoC level is presented in Fig. 44. Unlike OCV Mapping that has to apply two different OCV-SoC curves for charge and discharge, FNN is capable of handling SoC estimation for either charge or discharge with a single model, while also obtaining more precise results.
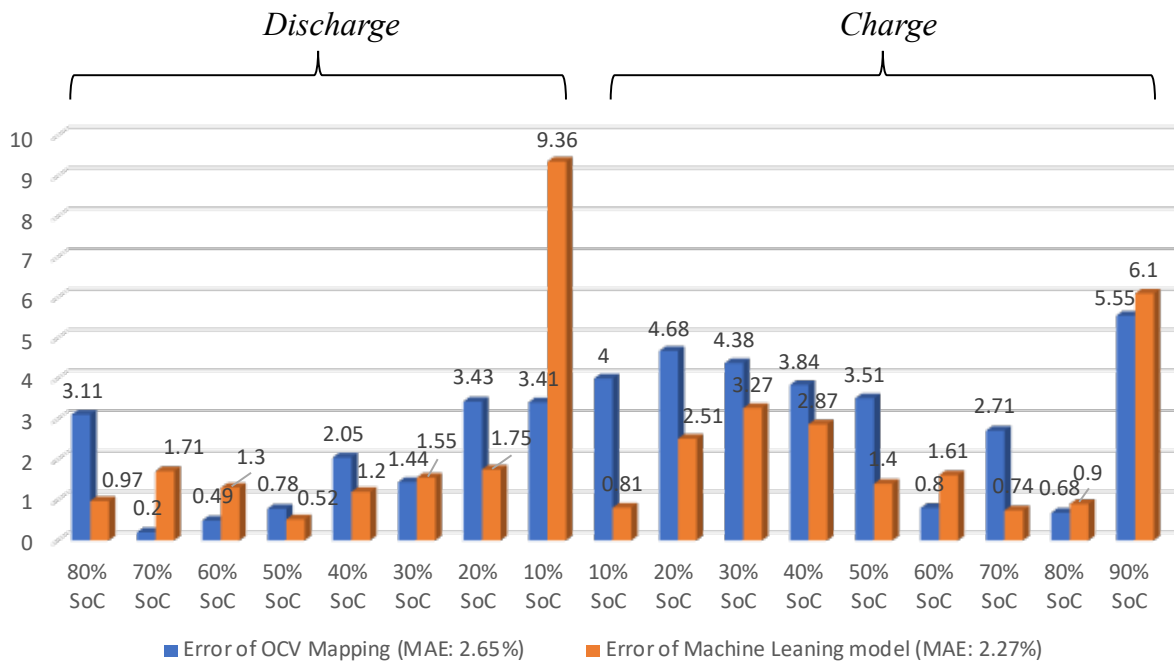

Figure 43: Average Error of OCV Mapping and machine learning-based approach at each SoC level for both charge and discharge.

Appendix B

The robustness of the FNN has been tested with the oscillated voltage response, a comparison between oscillated input and stable input was made to evaluate the performance of this model. Figure 44 illustrates three voltage inputs at 30% SoC level during charge, one of which is oscillated due to a manually set changing variable. Based on the MAEs shown in the figure, this FNN provided a consistently accurate result even if the input is drastically changed by artificial disturbance.
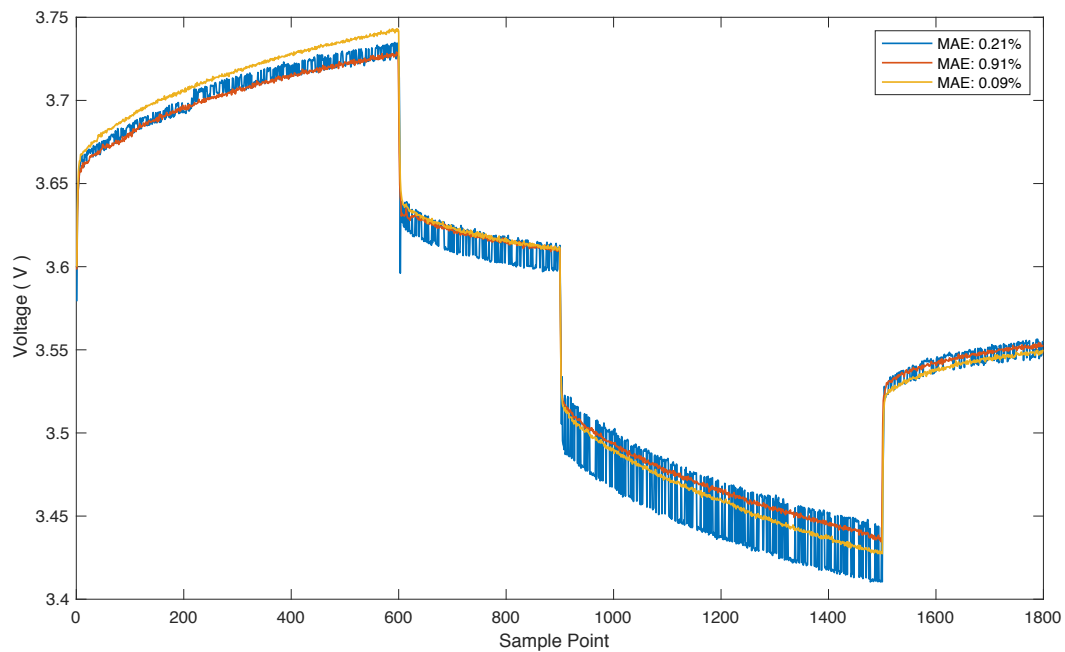

Figure 44: Sample inputs at 30% SoC.